Acta Biomaterialia 190 (2024) 362–378

Contents lists available at ScienceDirect

Acta Biomaterialia

journal homepage: www.elsevier.com/locate/actbio

Full length article

Machine learning reveals correlations between brain age and mechanics

Mayra Hoppstädter[a], Kevin Linka[b], Ellen Kuhl[c], Marion Schmicke[d], Markus Böl[a,*]

[a] Institute of Mechanics and Adaptronics, Technische Universität Braunschweig, Braunschweig D-38106, Germany
[b] Institute of Continuum and Material Mechanics, Hamburg University of Technology, Hamburg D-21073, Germany
[c] Departments of Mechanical Engineering and Bioengineering, Wu Tsai Neurosciences Institute, Stanford University, Stanford, California USA
[d] Clinic for Cattle, University of Veterinary Medicine Hannover, Hannover D-30559, Germany

ARTICLE INFO

Article history:
Received 16 June 2024
Revised 30 September 2024
Accepted 3 October 2024

Keywords:
Brain tissue
Age dependency
Axial tension/compression experiments
Machine learning
Material modeling
Sus scrofa domesticus

ABSTRACT

Our brain undergoes significant micro- and macroscopic changes throughout its life cycle. It is therefore crucial to understand the effect of aging on the mechanical properties of the brain in order to develop accurate personalized simulations and diagnostic tools. Here we systematically probed the mechanical behavior of $n = 439$ brain tissue samples in tension and compression, in different anatomical regions, for different axon orientations, across five age groups. We used Bayesian statistics to characterize the relation between brain age and mechanical properties and quantify uncertainties. Our results, based on our experimental data and material parameters for the isotropic Ogden and the anisotropic Gasser-Ogden-Holzapfel models, reveal a non-linear relationship between age and mechanics across the life cycle of the porcine brain. Both tensile and compressive shear moduli reached peak values ranging from 0.4–1.0 kPa in tension to 0.16–0.32 kPa in compression at three years of age. Anisotropy was most pronounced at six months, and then decreased. These results represent an important step in understanding age-dependent changes in the mechanical properties of brain tissue and provide the scientific basis for more accurate and realistic computational brain simulations.

Statement of significance

In this paper, we investigate the age-dependent mechanical properties of brain tissue based on different deformation modes, anatomical regions, and axon orientations. Hierarchical Bayesian modeling was used to identify isotropic and anisotropic material parameters. The study reveals a nonlinear relationship between shear modulus, degree of anisotropy, and tension-compression asymmetry over the life cycle of the brain. By demonstrating the non-linearity of these relationships, the study fills a significant knowledge gap in current research. This work is a fundamental step in accurately characterizing the complex relationship between brain aging and mechanical properties.

1. Introduction

The central nervous system, consisting of the brain and spinal cord, is the control center of the human body. The brain contains about 86 billion nerve cells [1–3] that generate, receive and transmit signals [4–6]. Therefore, it is well protected within the cranial cavity and surrounded by cerebrospinal fluid. As a result, it is less exposed to mechanical stress than other organs. However, under pathological conditions, such stresses can occur. One example is traumatic brain injury (TBI), in which acceleration and impact cause contact between the brain and the skull, resulting in strains and stresses [7–10]. Another example is cancerous tissue, which has a different stiffness than healthy tissue, resulting in stiffness gradients [11–13]. Technological advances allow computer simulation of such pathological conditions [14–17] and neurosurgical treatments [18,19]. However, to make reliable statements based

* Corresponding author.
E-mail address: m.boel@tu-braunschweig.de (M. Böl).

https://doi.org/10.1016/j.actbio.2024.10.003

on these simulations, the material properties of brain tissue are needed.

Over the past 60 years, there has been great progress in material characterization [20]. Mainly in vitro experiments have been performed under a variety of deformation states, with different species and at different rates, to name a few. The results show agreement on non-linear, time-dependent [21–26], deformation-dependent [22,24,27–30], and region-dependent properties [22,28,31–35]. However, results regarding anisotropy are inconsistent, with some studies reporting isotropic [28,32,36,37] and others reporting anisotropic behavior [22,31,35,37–39]. A potential factor that has received less attention is the influence of the age of the specimens used. There is a wide variation in the literature, ranging from prenatal bovine tissue [40] to 94 year old human subjects [22].

The brain, more than other organs, undergoes major micro- and macroscopic changes during the life cycle. Within the developmental phase, the characteristic gyri and sulci form during the embryonic stage [41,42] and the brain increases in mass [43–45]. In the subsequent aging phase, beginning at 22 years of age, the brain again loses mass [44–46]. In vivo studies using magnetic resonance elastography (MRE) have linked these age-related changes to alterations in the mechanical properties of brain tissue. Studies of individuals aged 18–89 years consistently show a decrease in brain stiffness with age [46–50]. However, MRE studies focusing on the developmental phase in individuals aged 7–18 years found no significant variation in brain stiffness across this age range [51,52]. McIlvain et al. [53] extended this research by comparing brain stiffness between the developmental phase (12–14 years) and the early aging phase (18–33 years), reporting both increases and decreases in stiffness depending on the brain region examined. This regional dependence of age-related stiffness changes was further confirmed in a subsequent study covering an age range of 5 to 35 years [54]. In addition, diffusion tensor imaging (DTI) studies, which reveal microstructural orientation, have demonstrated a non-linear behavior of fractional anisotropy (FA) across the lifespan [55–57]. As these experiments are performed in vivo, only very small strain ranges can be analyzed. Thus, the full complexity of brain biomechanics cannot be captured. In vitro studies can capture the complexity, but reported results vary due to the lack of standardized test protocols.

The age dependence of brain tissue has been studied under indentation [34,37,58–63], uniaxial compression [22,28,31], uniaxial tension [22,28], and shear [22,28,31,33,64]. Tissues from mice [37,63], rats [34,37,59–62], pigs [31,58,64], and humans [22,28,33] were used. To characterize changes over the lifespan, two [31,34,61,63,64] and five [62] age groups were compared, focusing on whether the brain stiffens or softens with age. Ex vivo studies predominantly indicate that brain stiffness increases with age during the developmental phase [37,62–64]. These findings are further supported by studies comparing brain tissue from the developmental phase with that from the aging phase, which also show an increase in stiffness [33,34,60]. However, there are conflicting results within the developmental phase, with some studies reporting a softening of the brain tissue with age [31,58,59]. In addition, studies that have examined only the aging phase of the brain life cycle report no significant age-related changes in stiffness [22,28].

In addition to the inconsistent results, the current state of the art shows a lack of data on the influence of age on the aforementioned region and deformation dependence, such as the tension-compression asymmetry (TCA). Furthermore, it remains unclear whether and to what extent the non-linear development of FA over the lifespan [55,56] affects the mechanical anisotropy, as there are no studies that have investigated the axon orientation-dependent behavior for different age groups. Budday and Kuhl [45] proposed a linear description of the Ogden material parameters as a function of FA and age. However, the study is based on in vivo results and shows no validation of the proposed description with existing experiments. In addition, the linear considerations of mechanical stiffness over the life cycle in the literature may not be sufficient as brain mass evolves non-linearly [43–45].

To date, there is no precise description of the relationship between age and brain stiffness measured in vitro. Therefore, in the present study, we used machine learning to learn the relationship based on experimental data. Recently, machine learning has been successfully used for image segmentation to identify brain tumors [65–67] or Parkinson's disease [68]. In addition, machine learning has been used to predict brain age based on gene signatures [69,70], MRE [71], and electroencephalography data [72]. In the context of biomechanics, probabilistic approaches such as Bayesian inference have been used to quantify the uncertainty of constitutive material parameters [73–77]. In addition, the studies of Liang et al. [78] and Linka et al. [79] used convolutional neural networks (CNNs) and constitutive artificial neural networks (CANNs) to link the mechanical behavior to the underlying microstructure to obtain a more accurate prediction of constitutive models. However, both approaches were performed without considering the effects of aging.

The present study attempts to fill the gap of accurately describing the relationship between brain age and mechanical properties. Therefore, data-driven learning was applied to mechanically tested brain tissue. The age range of the tissue samples covers both the developmental and early aging phases of the brain. The tissue was mechanically tested under uniaxial tension and compression, taking into account region and axon orientation dependence. The results were then evaluated using Bayesian hierarchical modeling to determine the evolution of material properties over time.

2. Materials and methods

2.1. Ethical approval

The tissue was exempt from review by the ethics committee according to national regulations (German Animal Welfare Act) because the brains were obtained from healthy domestic pigs in a slaughterhouse immediately after sacrifice. An exception is the first age group, for which animals from a collaboration with the Martin Luther University Halle-Wittenberg and the University of Veterinary Medicine Hanover were used. The brains were removed after the animals had been euthanized (H1-2/T1-20, TiHo-T-2018-24).

2.2. Tissue sample preparation and processing

In this study, experiments were performed on forty-two ($n = 42$) brains from pigs (*Sus scrofa domestica*). Pig brain tissue was used because it is very similar to human brain tissue and [80,81], and because it is readily available fresh. To ensure safe transport of the brains without damage, they were stored in the skull and transported to the laboratory within a very short time after the animal was sacrificed. Upon arrival, the brains were removed, weighed and measured before being stored at 4 °C for a few minutes in preparation for sampling. Throughout processing, samples were hydrated with Dulbecco's phosphate buffered saline (DPBS). For the mechanical tests, samples were taken from four different anatomical regions: The gray matter cortex (CX), white matter regions including the corpus callosum (CC) and corona radiata (CR), and the basal ganglia (BG), which is a mixture of gray and white matter. The gray matter was assumed to have isotropic material properties based on previous studies [30], while we showed an anisotropic behavior of the white matter region CC under compression [82]. Therefore, CC samples were tested to investigate the

Table 1
Summary of the $n = 439$ experiments depending on the investigated region (cortex CX, basal ganglia BG, corpus callosum CC, and corona radiata CR), the orientation (0°, 45°, 90°) and the deformation state (uniaxial tension/compression).

deformation state	region	orientation	age group (age in months)				
			S_1	S_2	S_3	S_4	S_5
			2.5 ± 0.7	6.2 ± 0.4	36.0 ± 5.6	48.0 ± 3.5	64.3 ± 9.5
axial tension	BG	-	12	18	9	4	-
	CR	-	9	14	9	7	-
	CC	0°	12	18	12	-	3
subtotal			*33*	*57*	*30*	*11*	*3*
axial compression	CX	-	11	14	8	6	5
	BG	-	15	19	5	6	8
	CR	-	27	30	16	10	13
	CC	0°	13	14	5	11	4
	CC	45°	2	6	-	-	8
	CC	90°	14	15	8	6	6
subtotal			*82*	*98*	*42*	*39*	*44*
total			**115**	**155**	**72**	**50**	**47**

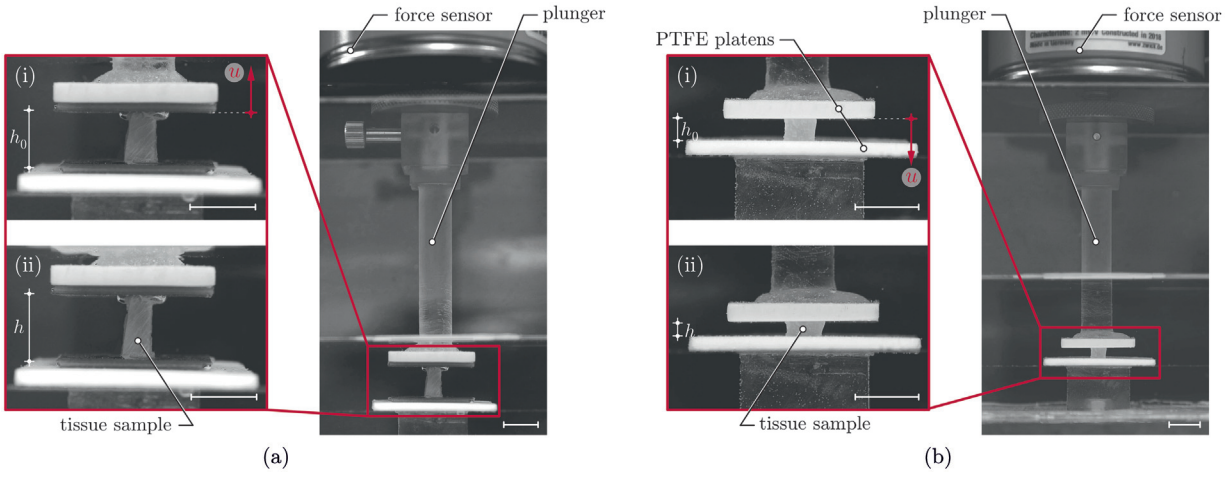

Fig. 1. Experimental setup for (a) axial tension and (b) axial compression experiments. Note that (i) and (ii) show the undeformed and deformed states, respectively. Scale bar: 10 mm.

influence of axon orientation on their mechanical properties over time.

First, the brains were separated into two hemispheres by careful sectioning along the sagittal plane. Using a custom-made cutting tool with siliconized microtome blades to prevent the samples from sticking together, a total of 439 cubic samples were collected at equidistant intervals of 4 mm. The samples were obtained from animals aged 65 days (S_1), 175 days (S_2), and between 854 and 2051 days. The latter were divided into three age groups ($S_{3/4/5}$) at approximately one year intervals to ensure uniform coverage of the third to sixth years. Table 1 lists the number of samples per age group for each anatomical region, axon orientation, and deformation state.

2.3. Mechanical experiments

The experiments were performed according to Hoppstädter et al. [82] using two axial testing machines (Zwick Z0.5, Zwick GmbH & Co. Ulm, Germany) equipped with load cells of 2 N and 5 N, respectively, see Fig. 1. Regardless of the deformation state, all experiments were displacement controlled and performed at a quasi-static deformation rate of 0.05 %/s. During the experiments, a camera positioned in front of the samples provided real-time monitoring (at 5 Hz) to ensure proper performance (e.g. checking for proper contact between the top plate/plunger and the tissue). The camera had a resolution of 2048 × 2048 pixels. In addition, physiological conditions were mimicked by performing the experiments in transparent basins filled with 37 ± 2 °C tempered DPBS solution. To minimize the effects of tissue degradation, all experiments were performed within 18 h post mortem.

2.3.1. Axial tension experiments

For the axial tensile test (index: at), one hundred and thirty-four samples ($n = 134$, Table 1) were attached to the upper stamp and ower plate with superglue (Loctite® 406, Henkel Ireland Operations and Research Ltd. Dublin, Ireland). Both the stamp and the plate were coated with sandpaper (320 grit) to improve adhesion. To ensure proper adhesion, one side of the sample was first glued to the sandpaper of the lower plate, then the upper stamp was lowered to glue the opposite side of the sample to the stamp. After a drying time of 120–180 seconds, the samples were immersed in tempered DPBS solution in a dish to ensure the target temperature of 37 °C. Finally, the stamp was raised to the original sample height (measured prior to glueing) and the mechanical test was initiated. The test setup is shown in Fig. 1. The displacement of the upper platen u was predetermined, while the resulting force F was measured and used to calculate the mean engineering stress via $P = F/A_{at}$, where A_{at} is the axial cross-sectional area. The axial cross-sectional area was determined by measuring a digital image of the specimen taken before the test. The tensile stretch

$\lambda_{at} = 1 + u/h_0$ was calculated from u and the undeformed specimen height h_0, cp. Fig. 1. All experiments were performed up to $\lambda_{at} = 1.5$ or until tissue failure.

2.3.2. Axial compression experiments

Three hundred and five ($n = 305$) samples were subjected to orientation dependent (0°, 45°, 90°) axial compression tests (index: ac). Fiber orientation was determined as the angle between the fiber and the applied load direction. To reduce the influence of friction, polytetrafluoroethylene (PTFE) plates were attached to the top custom lightweight stamp and to the bottom plate. The engineering stress $P = F/A_{ac}$ was calculated by dividing the measured force F by the cross-sectional area A_{ac} of the undeformed sample. The compressive stretch λ_{ac} was determined by subtracting the displacement u of the upper stamp from the undeformed specimen height h_0, cp. Fig. 1(b).

2.4. Data processing

The raw force-displacement data was acquired at a frequency of 10 Hz and stored for later analysis. To avoid potential distortion during post-processing, the raw data was smoothed based on the noise level in the acquired data. The smoothing process was performed by calculating the average value over 5% strain for axial tension and 4% strain for compression (function *smooth*, MATLAB®R2019b, The MathWorks, Inc.). The origin of the force was determined as the point where the punch first contacted the tissue sample. To determine this point, a post-processing step was performed based on the camera and force-displacement data. The contact point was identified as the moment when the specimen underwent transverse stretching (axial compression) accompanied by a noticeable change in the force signal. For the tension tests, the origin of the force was determined by the initial specimen height measured optically before the test. To determine the elastic regions of the force-displacement curves, the tangents $\mathcal{T}_i$ were calculated by finite differences at the points u_i, $i = 1, 2, \ldots, m$, where m is the maximum number of measurement points. The elastic region of the curve was defined as the section in which the slope increases monotonically, or is at least constant, i.e. $\mathcal{T}_{i+1} \geq \mathcal{T}_i$. The end point of the elastic range was identified as the point u_j where $\mathcal{T}_{j+1} < \mathcal{T}_j$. In general, measurements were excluded from the analysis if operational problems occurred, such as sample slippage under compression or no force development despite contact, and incomplete sample adhesion under tensile loading.

3. Continuum mechanical framework of brain tissue modeling

3.1. Kinematics

Following general principles of continuum mechanics, we introduce $\mathcal{B}_0$ and $\mathcal{B}$ as the reference and current configurations of a body, where the position of the particle is given by the vectors $\boldsymbol{X}$ and $\boldsymbol{x} = \boldsymbol{\varphi}(\boldsymbol{X})$, respectively. The non-linear mapping of a material particle from the reference configuration to the current configuration is represented by $\boldsymbol{\varphi}(\boldsymbol{X}, t)$ and the corresponding deformation gradient

$$\boldsymbol{F} = \frac{\partial \boldsymbol{x}}{\partial \boldsymbol{X}} = \nabla_X \boldsymbol{\varphi}(\boldsymbol{X}, t). \tag{1}$$

The Jacobian $J = \det \boldsymbol{F} > 0$ represents the volume change of the material particle and $\nabla_X(\bullet)$ is the spatial derivative according to the reference coordinates.

Taking into account the anisotropic behavior of the tissue material, we introduce the fiber direction vector $\boldsymbol{M}$ and the corresponding structure tensor

$$\boldsymbol{Z} = \boldsymbol{M} \otimes \boldsymbol{M} \tag{2}$$

into the reference configuration. The corresponding muscle fiber stretch

$$\lambda^2 = I_4 = \boldsymbol{C} : \boldsymbol{Z} \tag{3}$$

depends on the right Cauchy-Green tensor $\boldsymbol{C} = \boldsymbol{F}^T\boldsymbol{F}$ and is related to the fourth invariant I_4.

Finally, the corresponding scalar-valued first invariant

$$I_1 = \mathrm{tr}\boldsymbol{C} \tag{4}$$

represents an isotropic measure of isotropic material characteristics.

3.2. Constitutive modeling of brain tissue

As experimental studies have shown [82], some tissue regions of the brain are characterized by isotropic mechanical material properties, while other regions are characterized by anisotropic properties. Accordingly, an isotropic and an anisotropic energy function are proposed below according to these regions.

To describe the isotropic tissue components of the brain, the Ogden (index: OGD) material model [83] in terms of the free energy

$$\Psi_{OGD} = \sum_{i=1}^{n} \frac{\widehat{\mu}_i}{\alpha_i}\left(\lambda_1^{\alpha_i} + \lambda_2^{\alpha_i} + \lambda_3^{\alpha_i} - 3\right) \text{ with } i = 1, 2, \ldots, n \tag{5}$$

is proposed. Here, $\widehat{\mu}_i$ and α_i are material parameters and n defines the number of terms used. For the sake of interpretation, it is useful to introduce the classical shear modulus as a function of the material parameters as $\mu = \frac{1}{2}\sum_{i=1}^{n} \widehat{\mu}_i\alpha_i$.

With the classical shear modulus and $\alpha = \alpha_i$ the strain energy function of the one-term Ogden model can be reformulated as follows

$$\Psi_{OGD} = \frac{2\mu}{\alpha^2}\left(\lambda_1^{\alpha} + \lambda_2^{\alpha} + \lambda_3^{\alpha} - 3\right). \tag{6}$$

Based on the energy function, the first Piola-Kirchhoff stress tensor for an incompressible tissue reads

$$\boldsymbol{P}_{OGD} = \frac{\partial \Psi_{OGD}}{\partial \boldsymbol{F}} - p\boldsymbol{F}^{-T} = \sum_{i=1}^{3} \frac{1}{\lambda_i}\frac{\Psi_{OGD}}{\lambda_i}(\boldsymbol{F}\boldsymbol{N}_i) \otimes \boldsymbol{N}_i - \frac{1}{\lambda_i}p. \tag{7}$$

Herein, the orthonormal vectors $\boldsymbol{N}_i$ denote the principal referential axes of stretch, p is a Lagrange multiplier and

$$\frac{\Psi_{OGD}}{\lambda_i} = 2\mu\frac{\lambda_i^{\alpha-1}}{\alpha}. \tag{8}$$

In contrast to the isotropic material response, the anisotropic tissue response is described by the Gasser-Ogden-Holzapfel (index: GOH) material model [84]

$$\Psi_{GOH} = \Psi_{iso}(I_1) + \Psi_{ani}(I_1, I_4), \tag{9}$$

with a preferred material direction. The entire energy function is divided into an isotropic (Ψ_{iso}) and an anisotropic part (Ψ_{ani}).

While the elastic ground matrix of brain tissue with isotropic properties is characterized by the isotropic neo-Hookean material model

$$\Psi_{iso} = \frac{c}{2}(I_1 - 3) \tag{10}$$

depending on the material parameter c and the first strain invariant I_1, the anisotropic part of Eq. (9) is represented by

$$\begin{aligned}\Psi_{ani} &= \frac{k_1}{2k_2}\left[\exp\left\{k_2\left[I_4^*\right]^2\right\} - 1\right] \\ &= \frac{k_1}{2k_2}\left[\exp\left\{k_2[\kappa I_1 + (1 - 3\kappa)I_4 - 1]^2\right\} - 1\right]\end{aligned} \tag{11}$$

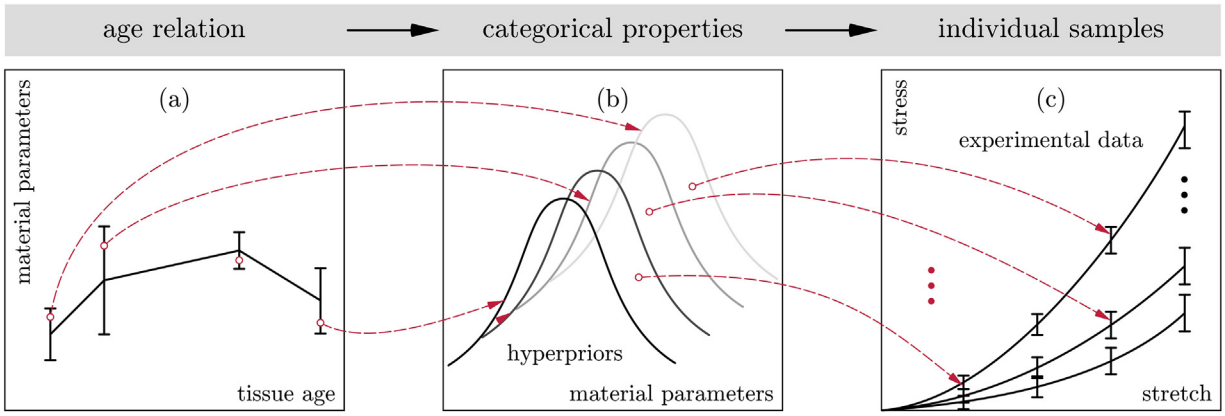

Fig. 2. Schematic representation of the Bayesian model hierarchy: (c) Representation of the mean experimental stress-strain curves with the standard deviation at certain points. This distribution is represented by the hyperpriors of the material parameters shown in (b), and the age relationship of these material parameters is shown in (a).

and depends on the first and fourth invariants and is parameterized by the two material constants k_1 and k_2. The degree of anisotropy is quantified by κ (also called dispersion parameter) and describes the rotationally symmetric density around the preferred material direction $\boldsymbol{M}$. Obviously, $\kappa = 1/3$ represents the ideal isotropic case, while $\kappa = 0$ represents the perfect transverse isotropic case.

Finally, the first Piola-Kirchhoff stress tensor

$$\begin{aligned}\boldsymbol{P}_{\mathrm{GOH}} &= 2\boldsymbol{F}\frac{\partial \Psi_{\mathrm{GOH}}}{\partial \boldsymbol{C}} - p\boldsymbol{F}^{-T} \\ &= 2\boldsymbol{F}\left[\frac{\partial \Psi_{\mathrm{GOH}}}{\partial I_1}\boldsymbol{I} + \frac{\partial \Psi_{\mathrm{GOH}}}{\partial I_4}\boldsymbol{M}\otimes\boldsymbol{M}\right] - p\boldsymbol{F}^{-T},\end{aligned} \tag{12}$$

can be expressed by the strain-energy function for an incompressible tissue with the derivatives

$$\frac{\partial \Psi_{\mathrm{GOH}}}{\partial I_1} = \frac{c}{2} + \kappa \quad \text{and} \quad \frac{\partial \Psi_{\mathrm{GOH}}}{\partial I_4} = (1-3\kappa)\frac{\partial \Psi_{\mathrm{ani}}}{\partial I_4^*} \tag{13}$$

and $\boldsymbol{I}$, to be the second order identity tensor.

3.3. Bayesian modeling

Given the overall goal of the study to infer the temporal evolution of age-specific mechanical properties of tissues, we use Bayesian inference. To avoid overfitting, it is assumed that the mechanical properties of interest can be drawn from a distribution that evolves piecewise linearly over time for all measured specimens. Taking into account the variability of each measured specimen and using the properties of the entire cohort for each specific age group, a hierarchical modeling scheme is applied.

It is assumed that the material parameters from Eqs. (5) and (9) are drawn from lognormal prior distributions

$$\log\left(b_i[t_j]\right) \sim \mathcal{N}\left(f^p[t_j], \sigma_i^p[t_j]\right) \;\text{ with }\; b \in \{\mu,\, \alpha\},\, j = 1, 2, \ldots, t_n, \tag{14}$$

for each subject i, where b are the material parameters for the material model, t_n is the number of age bins analyzed, and σ_i^p are the individual standard deviations. Accordingly, the hyperprior distributions are taken directly at discrete time points and serve as hyperparameters in Eq. (14), as shown schematically in Fig. 2.

3.4. Parameter estimation

To analyze the age-specific evolution of the mechanical properties of brain tissue, we determined the model parameters of the isotropic OGD model and an anisotropic GOH model for different deformation cases. In particular, we considered uniaxial stretch in tension ($\lambda > 1$) and compression ($\lambda < 1$). Due to the symmetry and the assumed incompressibility, the lateral stretches in the isotropic case are $\lambda_2 = \lambda_3 = \lambda^{-1/2}$. The matrix of the deformation gradient components can thus be expressed as $[\boldsymbol{F}] = \mathrm{diag}[\lambda,\ \lambda^{-1/2},\ \lambda^{-1/2}]$. Applying this special form of the deformation gradient to Eq. (7) and adopting a one-term formulation for brain tissue [28], the nominal stress in the loading direction is obtained as

$$P_{\mathrm{OGD},11} = \frac{2\mu}{\alpha}\left(\lambda^{\alpha-1} - \lambda^{-\alpha/2-1}\right), \tag{15}$$

where the Lagrange multiplier has been eliminated by applying $P_{22} = P_{33} = 0$. For the anisotropic material characterization, only a rotationally symmetric dispersion around the mean axon direction $\boldsymbol{M}$ is used, defined by the unit vector $\boldsymbol{M} = \cos^2\vartheta\,\boldsymbol{e}_1 + \sin^2\vartheta\,\boldsymbol{e}_2$ with the orientation angle ϑ, where three different cases are distinguished, first, the axon orientation is aligned with the load direction (denoted as 0°), second, the axion orientation is orthogonal to the load direction ($\vartheta = 90°$), and third, the axon orientation is in between with $\vartheta = 45°$. Based on this, the deformation gradient matrix can be expressed as $[\boldsymbol{F}] = \mathrm{diag}[\lambda_1,\ \lambda_2,\ \lambda_2]$, giving the non-zero components of the Eq. (9) as

$$\begin{aligned}P_{\mathrm{GOH},11} &= \left[c + 2\left(\kappa + (1-3\kappa)\cos(\vartheta)^2\right)\frac{\partial \Psi_{\mathrm{ani}}}{\partial I_4^*}\right]\lambda_1 - p/\lambda_1, \\ P_{\mathrm{GOH},22} &= \left[c + 2\left(\kappa + (1-3\kappa)\sin(\vartheta)^2\right)\frac{\partial \Psi_{\mathrm{ani}}}{\partial I_4^*}\right]\lambda_2 - p/\lambda_2, \quad \text{and} \\ P_{\mathrm{GOH},33} &= \left[c + 2\kappa\,\frac{\partial \Psi_{\mathrm{ani}}}{\partial I_4^*}\right]\lambda_3 - p/\lambda_3.\end{aligned} \tag{16}$$

The stress response $P_{\mathrm{GOH},11}$ with respect to λ_1 and the material parameters (c, k_1, k_2, κ) can be determined with the conditions $P_{22} = P_{33} = 0$ and the incompressibility condition $\lambda_1\lambda_2\lambda_3 = 1$. The resulting material parameter sets are $\boldsymbol{\theta}_{\mathrm{OGD}} = \{\mu,\ \alpha,\ \sigma_{\mathrm{OGD}}\}$ and $\boldsymbol{\theta}_{\mathrm{GOH}} = \{c,\ k_1,\ k_2,\ \kappa,\ \sigma_{\mathrm{GOH}}\}$ for the isotropic and anisotropic material models, respectively, were estimated using Bayesian inference via Markov Chain Monte Carlo (MCMC). The MCMC algorithm allows us to sample efficiently from the posterior distribution, even for high-dimensional and complex models [85,86]. Here, $\sigma_{(\bullet)}$ [with $(\bullet)$ *in* {OGD, GOH}] represents the width of the probability $\pi\left(P_{(\bullet)}(\lambda)|\theta\right)$ between the measured $P_{\mathrm{exp}}(\lambda)$ and the modeled $P_{(\bullet)}(\lambda)$ stress-stretch relationships. To estimate representative mechanical quantities of brain tissue across different age categories,

we apply hierarchical modeling so that the well-known Bayes' theorem reads

$$\pi\left(\theta_{(\bullet)}, \phi | P_{\text{exp}}\right) = \frac{\pi\left(P_{\text{exp}}|\theta_{(\bullet)}, \phi\right)\pi\left(\theta_{(\bullet)}, \phi\right)}{\pi\left(P_{\text{exp}}\right)} = \frac{\pi\left(P_{\text{exp}}|\theta_{(\bullet)}\right)\pi\left(\theta_{(\bullet)}|\phi\right)\pi\left(\phi\right)}{\pi\left(P_{\text{exp}}\right)}, \tag{17}$$

where $\pi\left(\theta_{(\bullet)}|\phi\right)$ represent the prior distributions drawn from the hyperpriors $\pi(\phi)$. In addition, one must define the probability quantifying the similarity between the model output $P_{(\bullet)}$ and the corresponding measurement data P_{exp}, here postulated by a Student's t-distribution to stabilize the MCMC procedure against outliers [87], as

$$\pi\left(P_{\text{exp}}|\theta_{(\bullet)}, \phi\right) = \prod_{j=1}^{t_n}\prod_{i=1}^{s_n} \text{StudentT}_{\nu=4}\left(P^{t_j}_{(\bullet),i}\left[\ \theta_{(\bullet)}, \phi\right], \sigma_i\right), \tag{18}$$

where s_n represents the number of available tissue samples in the corresponding age class. Finally, the Eq. (17) can be solved numerically using the NO-U-Turn Sampler (NUTS) [88], a self-tuning version of the Hamiltonian Monte Carlo sampling algorithm [89], implemented in the Python package PyMC3 [90]. We used two chains, and the first 500 samples are used to tune the sampler and are discarded later. For the anisotropic GOH model, 2500 samples were used to tune the sampler. The subsequent 4000 samples define the posterior distributions of the parameters $\theta_{(\bullet)}, \phi$. From the converged posterior distribution, several parameter combinations were selected that well describe the temporal evolution of the reported cases. These posterior samples make it possible to quantify the coefficient of variation R^2 in each of these parameters based on the reported data.

4. Results

4.1. Mechanical behavior

4.1.1. Axial tension responses

The stress-stretch results of the tensile tests are shown in Fig. 3 with respect to the anatomical regions (BG, CC, CR), axon orientation and age. Irrespective of region and age, the brain tissue shows a non-linear, root-shaped stress-strain behavior that differs from that under axial compression, see Fig. 4. The mean and standard deviation are plotted up to the maximum elastic stretch $\lambda_{\text{at,max}}$ up to which none of the specimens failed in the respective anatomical region. A Table 6 listing the latter and the corresponding maximum stresses $P_{\text{at,max}}$ can be found in the Appendix. The standard deviations increase with increasing stress for all curves and the coefficients of variation (CV) are less than 81.7%. To compare the different age groups, Table 2 shows the tensile stresses in relation to the minimum elastic stretch $\lambda_{\text{at,min}}$ per age group for the respective anatomical regions. The latter are 1.046, 1.044 and 1.060 for the different regions BG, CC and CR, respectively. The BG region shows the stiffest response in the age group S_2 with a mean stress of 0.086 kPa and the softest in S_4 with a 52.3% smaller value of 0.041 kPa. Focusing on the time dependence, there is an increase in mean stress of 79.2% from S_1 to S_2, followed by a continuous decrease in stress up to S_4. In contrast, the stiffest response of the CR region is in the age group S_1 with 0.087 kPa. However, this region shows only small temporal variations, with a maximum difference of 18.4% between age groups S_1 and S_2. For the region $CC_{0°}$, the age group S_3 shows the highest mean stress of 0.142 kPa. Up to this age, there is a significant increase of 140.7%, followed by a decrease of 81.0%. This behavior indicates a non-linear evolution of stiffness over the considered age groups.

4.1.2. Axial compression responses

In addition to the axial tension experiments in Section 4.1.1, compression experiments were performed for the three anatomical regions CX, BG, and CR as a function of tissue age ($S_{1/2/3/4/5}$) up to a maximum compressive stretch of $\lambda_{\text{ac,max}} = 0.55$. The results in the form of stress-strain curves are shown in Fig. 4. The tissue shows non-linear, exponential behavior that varies with age and region. In addition, it can be seen that the highest variability occurs at maximum stretch.

Table 3 lists the corresponding stress values $P_{\text{ac,max}}$ at maximum stretch depending on the anatomical regions and age groups. Overall, the CVs are between 15.3% and 57.3% for BG and CR regions in S_3 and S_4, respectively. For the gray matter region CX, the highest load is found in the age group S_5 with 1.89 kPa. Comparing the development across all age groups considered, the CX region shows an increase in stress of 180% from S_1 to S_3, followed by a slight decrease of 12.5% to S_4 and a further increase of 107.7%. In addition, the BG region shows a similar trend over age, but with the highest stress of 1.31 kPa for S_3. The CR region, on the other hand, remains almost constant until S_4, with differences between the age groups of less than 15.3%. Here, the age-dependent stress maximum of 1.64 kPa occurs in S_4, followed by a decrease to 1.25 kPa in S_5.

4.1.3. Anisotropic behavior of the brain tissue

Of all the brain regions examined in this study, the CC region exhibits anisotropic material behavior due to the axon distribution. To investigate this in more detail, Fig. 5 shows the compressive stress-stretch relationships as a function of axon orientation (0°, 45°, 90°) and tissue age ($S_{1/2/3/4/5}$). In general, the stress-stretch behavior at the CC region, like the isotropic regions (CX, BG, CR) in Fig. 4, shows a nonlinear, exponential material behavior with a varying gradient depending on the axon orientation. The maximum standard deviation occurs at the maximum stretch $\lambda_{\text{ac,max}} = 0.55$, with CVs between 17.5% and 82.8% for $CC_{45°}$ at S_1 and $CC_{0°}$ at S_3. Table 4 lists the corresponding maximum compression stresses $P_{\text{ac,max}}$, evaluated at maximum compression stretch $\lambda_{\text{ac,max}} = 0.55$. In the following, the stress values are compared as a function of axon orientation per age group in order to detect the anisotropy that changes with age. For all groups, the $CC_{90°}$ region, where the

Table 2
Tensile stresses at minimum elastic elongation as a function of the examined tissue region (BG, CC, CR), axon orientation and age ($S_{1/2/3/4/5}$).

set	$P_{\text{at,min}}$ [kPa]		
	BG	$CC_{0°}$	CR
S_1	0.048 ± 0.033	0.059 ± 0.035	0.087 ± 0.029
S_2	0.086 ± 0.038	0.065 ± 0.036	0.071 ± 0.031
S_3	0.060 ± 0.021	0.142 ± 0.116	0.083 ± 0.053
S_4	0.041 ± 0.015	-	0.074 ± 0.040
S_5	-	0.027 ± 0.010	-

Table 3
Compressive stresses $P_{\text{ac,max}}$ depending on the examined tissue region (CX, BG, CR) and age ($S_{1/2/3/4/5}$).

set	$P_{\text{ac,max}}$ [kPa]		
	CX	BG	CR
S_1	0.36 ± 0.17	0.59 ± 0.25	1.10 ± 0.56
S_2	0.59 ± 0.19	0.87 ± 0.27	0.98 ± 0.40
S_3	1.04 ± 0.31	1.31 ± 0.20	0.83 ± 0.44
S_4	0.91 ± 0.40	0.73 ± 0.26	1.64 ± 0.94
S_5	1.89 ± 1.07	0.84 ± 0.28	1.25 ± 0.66

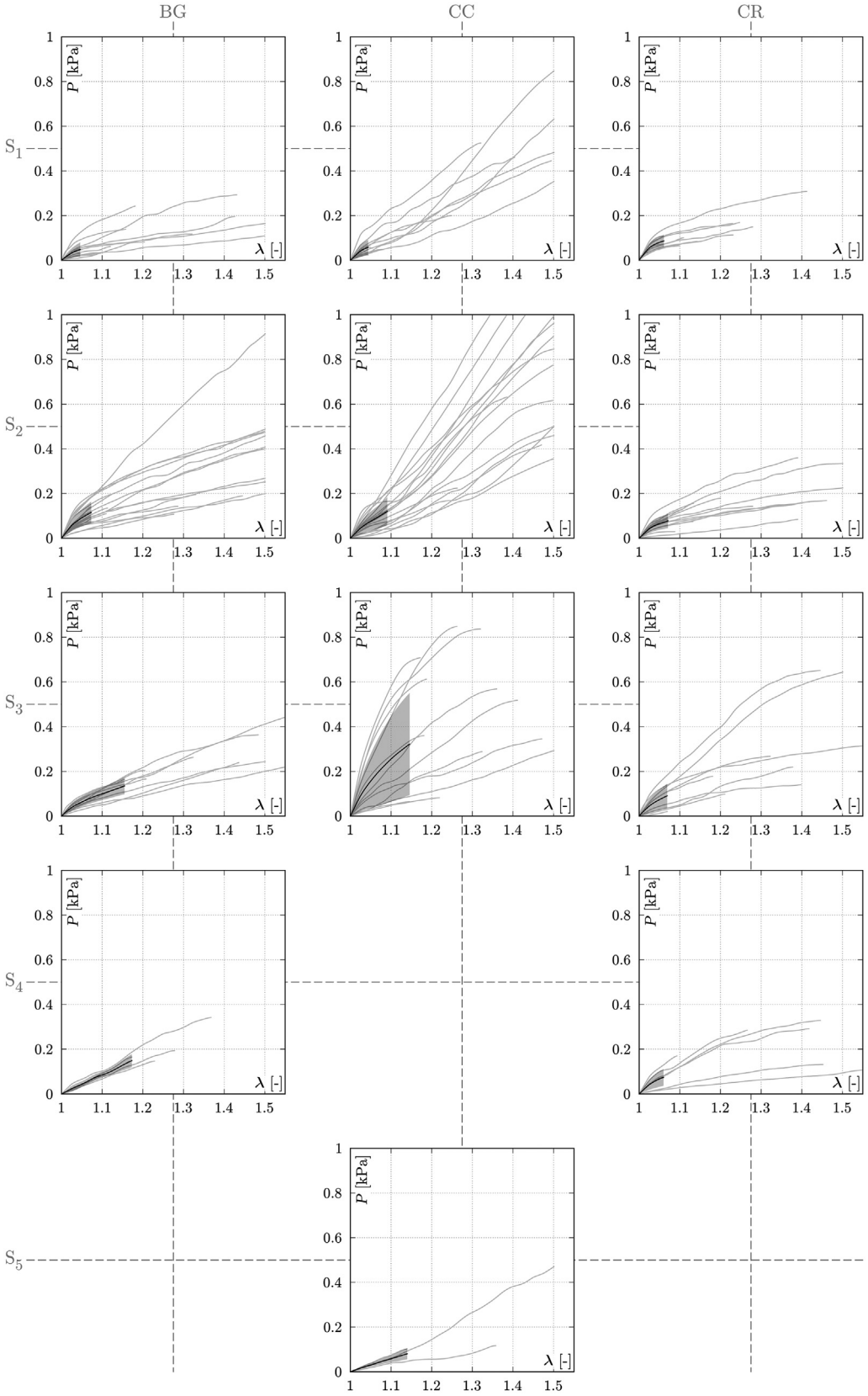

Fig. 3. Representation of the tension stress as a function of the examined region (basal ganglia BG, corpus callosum CC and corona radiata CR) and age group ($S_{1/2/3/4/5}$). Individual tests are highlighted in gray, the mean is highlighted in black, and the standard deviation is represented by the gray shaded areas. Note, the standard deviations are shown up to the smallest determined stretch in respective group. Figures are not shown for certain age groups and anatomical regions due to the unavailability of extracted samples for these specific cases.

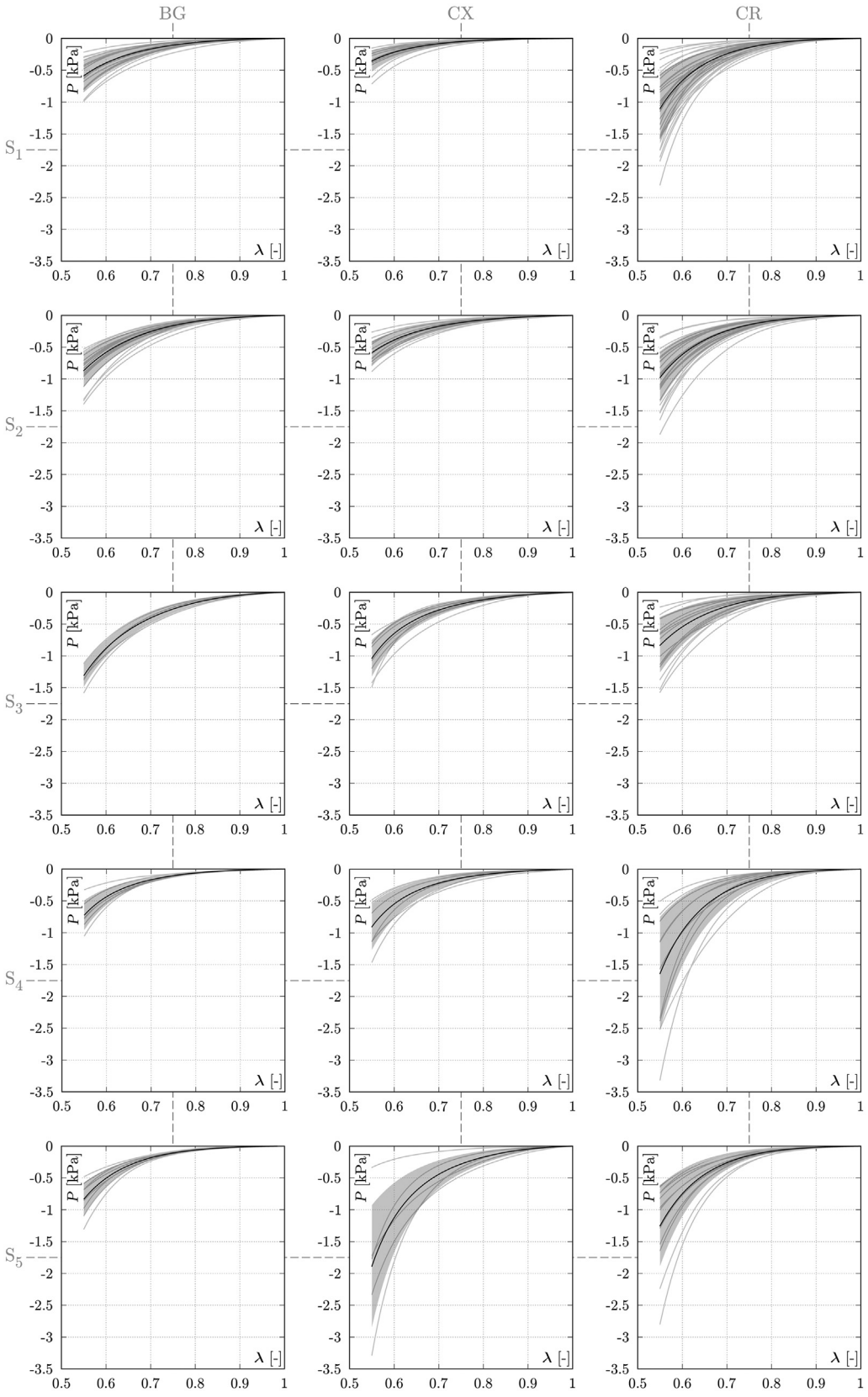

Fig. 4. Representation of the compressive stress as a function of the examined region (basal ganglia BG, cortex CX, and corona radiata CR) and age group ($S_{1/2/3/4/5}$). Individual tests are highlighted in gray, the mean is highlighted in black, and the standard deviation is represented by the gray shaded areas.

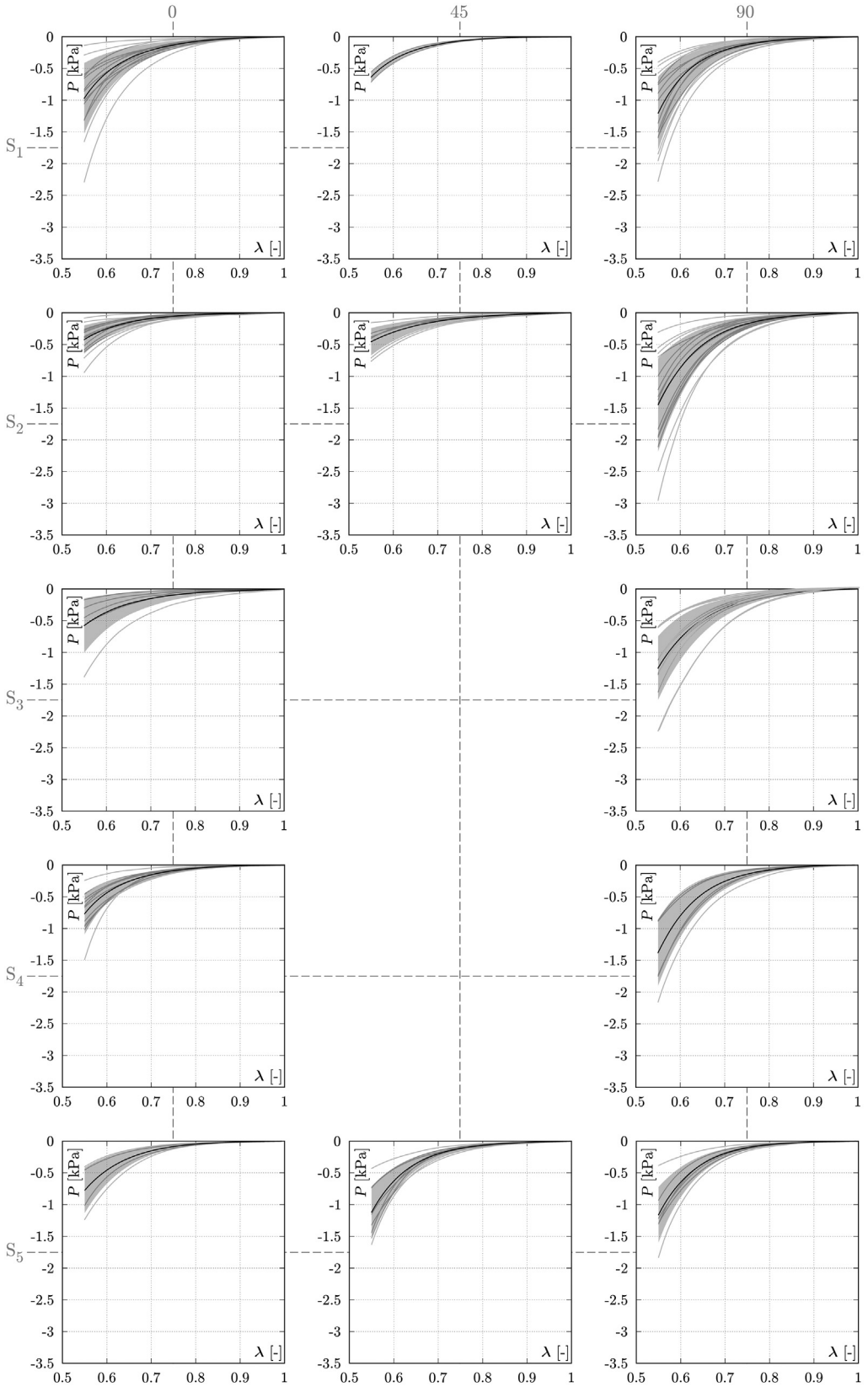

Fig. 5. Compressive stress-strain relationships of the CC region as a function of axon orientation and age. Individual tests are highlighted in gray, the mean is highlighted in black, and the standard deviation is represented by the gray shaded areas. Figures are not shown for certain age groups and anatomical regions due to the unavailability of extracted samples for these specific cases.

Table 4
Compressive stresses $P_{ac,max}$ of region CC evaluated at the maximum compressive stress $\lambda_{ac,max} = 0.55$ as a function of axon orientation (0°, 45°, 90°) and age ($S_{1/2/3/4/5}$).

set	$P_{ac,max}$ [kPa]		
	$CC_{0°}$	$CC_{45°}$	$CC_{90°}$
S_1	0.97 ± 0.58	0.63 ± 0.11	1.21 ± 0.60
S_2	0.42 ± 0.23	0.46 ± 0.24	1.45 ± 0.76
S_3	0.58 ± 0.48	-	1.25 ± 0.54
S_4	0.77 ± 0.34	-	1.38 ± 0.57
S_5	0.78 ± 0.41	1.12 ± 0.44	1.16 ± 0.48

Table 5
Tension-compression asymmetry in the form of the ratio between tensile and compressive stresses (P_{at}/P_{ac}) evaluated for $\lambda_{at,min} = 1.044$ as a function of the region investigated (basal ganglia BG, corpus callosum (CC) and corona radiata CR) and age ($S_{1/2/3/4/5}$).

set	P_{at}/P_{ac} [-]		
	BG	$CC_{0°}$	CR
S_1	5.9	7.5	9.7
S_2	8.9	20.6	7.7
S_3	4.2	9.7	7.0
S_4	6.3	-	7.9
S_5	-	6.8.	-

axons are under tensile stress, shows the stiffest response. However, the difference to the $CC_{0°}$ region changes with age, starting with a 24.7% higher stress in S_1 and reaching a maximum of 245.2% for S_2. From S_3 to S_5 the stress difference decreases from 115.5% to 48.7%. Comparing the regions $CC_{45°}$ and $CC_{90°}$, a similar trend can be seen, with the stress difference increasing from S_1 (92.1%) to S_2 (215.2%) and decreasing to S_5 (3.6%). In contrast, the orientation for $CC_{0°}$ shows a higher stress than for $CC_{45°}$ at S_1, but lower stresses at S_2 and S_5. This behavior indicates a non-linear trend in the anisotropy of CC over time.

4.1.4. Tension-compression asymmetry

Several soft biological tissues such as tendon [91,92], cartilage [93], bone [94], muscle [95–99], lung tissue [100], or cervical tissue [101,102] exhibit significantly different behavior under passive tensile and compressive loads, respectively, a property referred to as TCA. This also applies to brain tissue [22,24,35,82]. Regardless of the species considered and the direction of loading, it was found that the stress-strain reaction under tensile loading is up to 180 times greater than the reaction under compressive loading and changes during loading [82].

To further investigate the TCA of brain tissue in this study, we analyzed the ratio $P_{at}/|P_{ac}|$ between the magnitudes of tension P_{at} and compressive tissue stress $|P_{ac}|$. Fig. 6 shows the TCA as a function of absolute strain $|u/h_0|$ across different anatomical regions (BG, $CC_{0°}$, CR) and age groups. Overall, we observed a decrease in TCA ratio with increasing deformation, independent of age and region. However, further analysis of the age dependency, particularly at the minimum regional stretch $\lambda_{at,min} = 1.044$, reveals notable regional differences. These results, summarized in Table 5, highlight the age-dependent nature of TCA in brain tissue. For example, the BG shows a non-linear behavior in TCA across age groups, with the ratio P_{at}/P_{ac} ranging from a minimum of 4.2 in S_3 to a maximum of 8.9 in S_2. On the other hand, $CC_{0°}$ shows pronounced non-linearity, with a 175% increase in the ratio between S_1 and S_2 (from 7.5 to 20.6), followed by a 53% decrease to S_3 and a 30% decrease to S_4. In contrast, the CR shows an approximately constant level of TCA across the age groups S_2 to S_4. These results not only underscore the age-related changes in tissue stress, but also highlight the different levels of TCA in different regions of the brain. Understanding these variations is crucial to explaining the mechanical properties and behavior of brain tissue.

4.2. Age relations

The experimental results were estimated using the methods described in Section 3.4. The Ogden model was used for the isotropic regions CX, BG and CR with the deformation states uniaxial tension and compression. In the following, only the age dependence of the shear modulus is discussed in order to investigate the change in stiffness with age. The nonlinearity factor α can be found in Section A.3 of the Appendix.

Fig. 7 (a) shows the tensile shear modulus for the anatomical regions for the age groups. Fig. 7(b) shows the behavior of the shear modulus with time. Overall, satisfactory agreement between model and tensile tests was obtained with $R^2 = 0.81 \pm 0.17$ for BG, $R^2 = 0.92 \pm 0.07$ for CC 0°, and $R^2 = 0.67 \pm 0.11$ for CR. The highest variability, regardless of anatomical region, is found in the two oldest groups, reflecting the uncertainty caused by the smaller number of samples and the wider age range compared to S_1 and S_2. Consequently, the CVs in these two age groups range from 27.9% for the CR region (S_4) to 80.7% for the CC region (S_5). On the other hand, the maximum CV for the younger groups is 27.5%. It can be seen that the shear modulus of the BG region shows a non-linear behavior with age, with a maximum of 0.35 kPa at S_2. The response of the CR region, on the other hand, shows an almost constant behavior. The CC region of the white matter also shows a pronounced non-linear behavior with the highest shear modulus of 0.88 kPa at S_3, corresponding to an age of three years. These results are consistent with the experimental results of Section 4.1.1.

The shear moduli obtained for the uniaxial compression tests are shown in Fig. 8 as a function of the anatomical regions (CX, BG, CR) and the age groups $S_{1/2/3/4/5}$. The model response is in satisfactory agreement with the experimental data (region-dependent coefficients of determination $R^2 = 1.00 \pm 0.003$ for CX, $R^2 = 0.99 \pm 0.02$ for BG, and $R^2 = 0.99 \pm 0.008$ for CR). In addition, the shear modulus shows small CVs with a maximum of 39.3% for the CX region under age group S_5. This indicates a low uncertainty and thus a high confidence in the analyzed data. The shear modulus of the mixed gray/white matter region BG increases from S_1 (mean 0.14 kPa) to S_3 (mean 0.33 kPa). Thereafter, the shear modulus decreases to 0.11 kPa before increasing slightly to 0.15 kPa. In contrast, the shear modulus of the CR region remains almost constant from S_2 to S_5. However, the shear modulus of the CX region shows a similar trend to the BG region, with a low shear modulus of 0.06 kPa at S_1 and an increase of 100% from S_4 to S_5. This is also consistent with the results of the maximum experimental stresses from Section 4.1.2. These results indicate that the shear modulus behaves nonlinearly in time and independent of deformation state and anatomical region. This is consistent with the behavior of the maximum stresses shown in Section 4.1.2.

To investigate the influence of age on the mechanical anisotropy, the compression experiments of the CC region were fitted with the GOH model, see Section 3.4. Fig. 9 shows the dispersion parameter κ with a value of 1/3, corresponding to an isotropic behavior (dashed line). The model agrees well with the tests with a minimum of $R^2 = 0.99 \pm 0.01$. The dispersion parameter κ shows the highest variability of 34.6% within the age group S_1, which corresponds to an age of 2 months. The degree of anisotropy is highest in S_2 with an average factor of 0.24. Over time, κ decreases from S_1 to S_2 and increases again up to S_4 before decreasing again

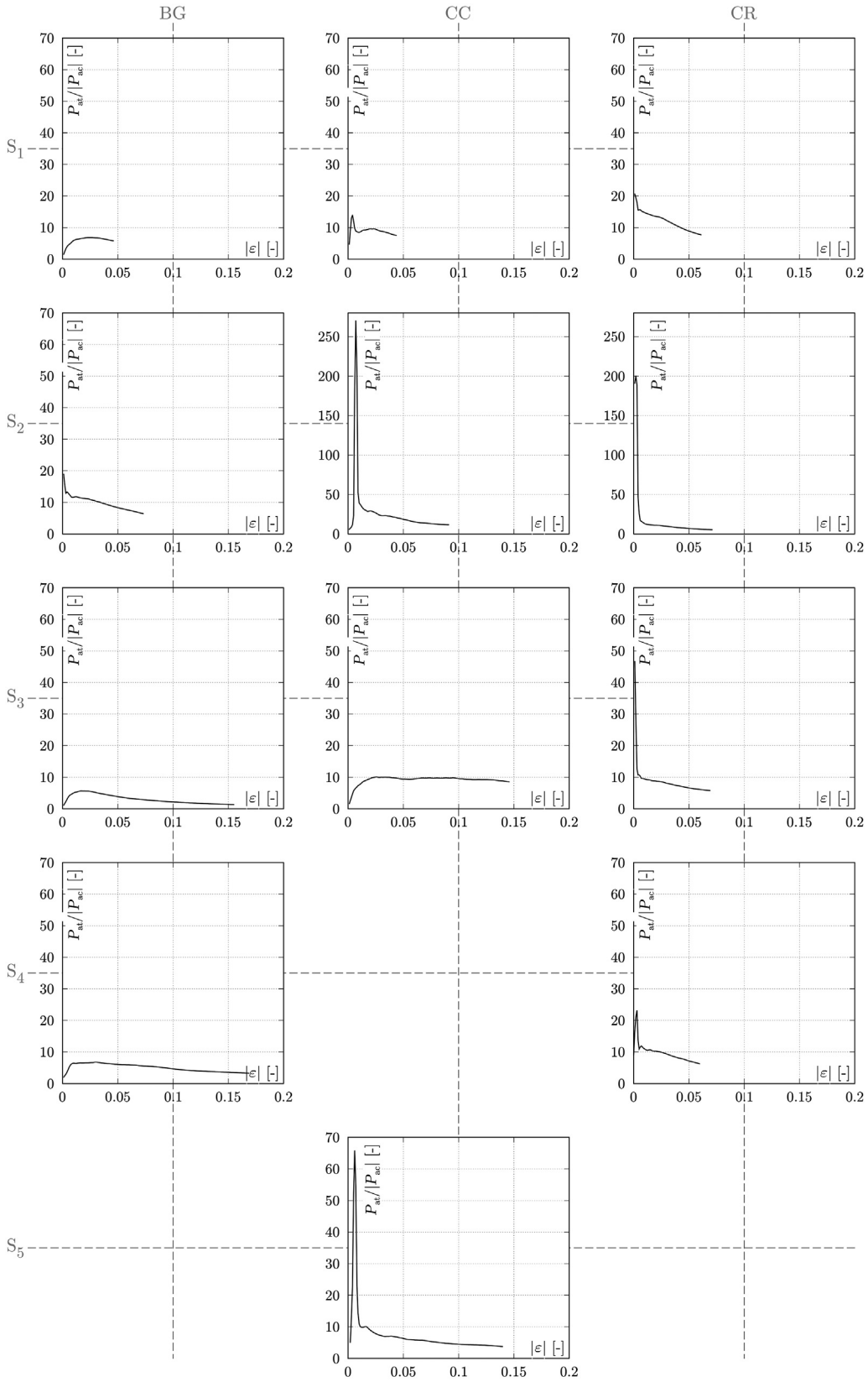

Fig. 6. Development of tension-compression asymmetry. Tensile-to-compressive stress ratio versus absolute strain for the regions BG, CC_{0°, and CR and age groups $S_{1/2/3/4/5}$. Figures are not shown for certain age groups and anatomical regions due to the unavailability of extracted samples for these specific cases.

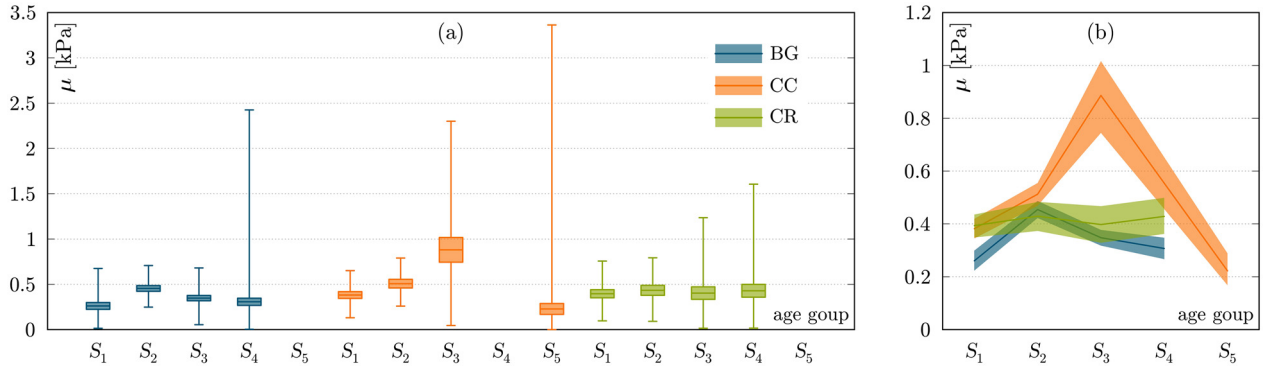

Fig. 7. Bayesian learning of the functional dependence between tissue stiffness and age for axial tension: (a) Hierarchically learned shear modulus distributions across tissue regions and age groups and (b) corresponding median of shear modulus (solid line) and percentiles (shaded areas), linearly interpolated across tissue age.

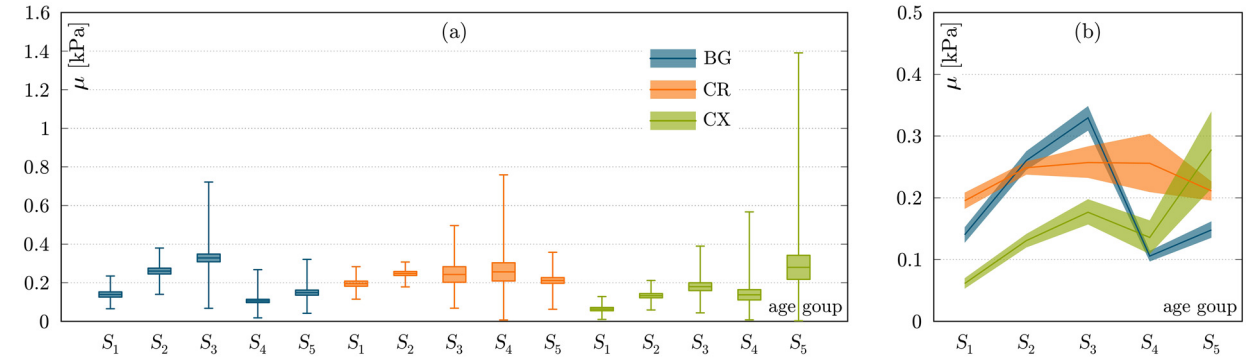

Fig. 8. Bayesian learning of the functional dependence between tissue stiffness and age for axial compression: (a) Hierarchically learned shear modulus distributions across tissue regions and age groups and (b) corresponding median of shear modulus (solid line) and percentiles (shaded areas) linearly interpolated across tissue age.

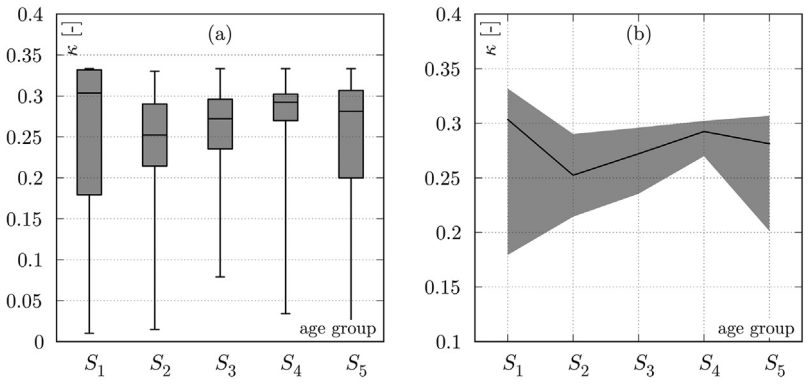

Fig. 9. Bayesian learning of the functional dependence between tissue anisotropy and age: (a) Hierarchically learned dispersion parameter (κ) for the tissue region CC and across five different age groups and (b) corresponding median dispersion parameter κ (solid line) and percentiles (shaded areas) linearly interpolated over the tissue age. Dashed lines indicate ideal tissue isotropy.

slightly. This result is consistent with the experimental results in Section 4.1.3.

5. Discussion

5.1. Age-dependent mechanical behavior

In the present study, in vitro experiments were combined with data-driven learning to accurately describe the mechanical behavior of brain tissue with age. Because it is important to understand the uncertainties in our data, Bayesian inference was used to fit the experimental results. This not only provided an accurate estimate of the mechanical properties, but also provided material parameters that are crucial for future investigations. Isotropic Ogden material parameters were generated for five age groups ranging from two to seventy-six months.

The analysis showed that the tensile properties of brain tissue change non-linearly with age, with clear differences observed in different anatomical regions. While the CR region shows an approximately linear behavior, the trend for the BG and CC regions could be described by a piecewise linear function. In the BG region, maximum stiffness is reached at 6 months (S_2) and in the CC

region at 3 years (S_3). So far, there is a lack of studies investigating the tensile behavior with age. Only Budday et al. [28] and Jin et al. [22] reported no significant age dependence in their tensile tests. However, both investigated human brain tissue aged 54 to 81 years [28] and 60 to 85 years [22]. Considering the developmental correlation between pigs and humans proposed by [64], a 1-year-old pig can be roughly compared to a 4-year-old human. Taking this into account, it becomes clear that the specimens of Budday et al. [28] and Jin et al. [22] represent higher ages than the present study. However, it should be noted that we observed an almost constant behavior of the shear modulus when comparing the two oldest groups. This suggests that changes in the tensile properties of the brain occur in the developmental phase before the age of 22 years, when brain mass begins to decrease [45].

In addition, we found that the compressive shear modulus exhibits regional and age-dependent behavior. The shear moduli of the BG and CX regions follow a non-linear trend with age, with maximum values at 3 years (S_3). Interestingly, both regions show a decrease in shear modulus from 3 to 4 years (S_3 to S_4), although this is more pronounced in the BG region. Between 4 and 5 years (S_4 to S_5), both regions show a slight increase in shear modulus. In the CR region, however, there is no age dependency and thus an almost constant behavior over time. For uniaxial compression, only the results of the studies by Budday et al. [28] and Jin et al. [22] can be considered for comparison. Both studies report no age dependence for their compression results. As with the tension stress results, this difference can be explained by the older age of the samples compared to the present study. Comparing the age groups S_4 and S_5 of the present study, only the CX region shows an increase in stiffness, but with a high variability in the data. The BG and CR regions show an almost constant shear modulus in these two groups. The conclusion from the tensile properties that the nonlinear behavior occurs mainly in the development phase also applies to the compression properties.

In addition, studies examining brain tissue under indentation [34,37,60,62,63] agree that stiffness increases with age. For example, Antonovaite et al. [63] compared the hippocampus and cerebellum of juvenile and adult mice and reported an increase in stiffness of 20–150% in the adult animals. The authors attribute this increase in stiffness to the relative area covered by astrocytes. Furthermore, studies on rat brain tissue also showed a significant increase in stiffness with age [34,60,62], with the exception of Gefen et al. [59]. The latter analyzed rat tissue from 13, 17, 43, and 90-day-old rats and reported a significant softening of the brain with age. However, this study examined a different stress state as the brain was left in the skull during the experiments and Elkin et al. [60] and Finan et al. [34] determined anatomical regions based on histological thin sections. The results of Gefen et al. [59] can be compared with those of Shulyakov et al. [62], who studied an age range from 1 to 180 days and also left the brain in the skull during the experiments. However, the latter reported a stiffening of the brain tissue after 21 days. This highlights the importance of a non-linear description of the mechanical properties of brain tissue, as we have shown in the underlying study. Our results show that either stiffening or softening is possible depending on the age groups compared. Therefore, further studies with a wide age range and for different animal species are needed.

Studies examining brain tissue under shear stress have also yielded contradictory results. While Chatelin et al. [33] and Thibault and Margulies [64] found increasing brain stiffness with age for tissue from the corona radiata, thalamus, brainstem, and mixed gray and white matter, Prange and Margulies [31] reported an opposite trend. However, they noted that this trend only holds for large deformations, as a comparison of their results for 2.5% shear strain with those of Thibault and Margulies [64] showed similar results. Another reason for the differences may be that Prange and Margulies [31] compared the mixed gray and white matter of the young group with the average of the individually tested gray and white matter of the adult group. Since we have shown that there is a significant anatomical dependence of the mechanical properties of brain tissue [82], comparing of mixed with specific regions may not be sufficient to isolate the effect of age dependence. Overall, most in vitro studies report an increase in stiffness with age, which is consistent with our study for the BG and CX anatomical regions. None of the aforementioned studies examined the CR region.

In vivo studies using MRE to investigate age-related changes in brain stiffness consistently report a decrease in stiffness with age and focus primarily on individuals aged 18–89 years [46–49]. Thus, these studies predominantly address the aging process rather than early development. In contrast, our study focused on the brain development and early aging. Interestingly, MRE studies examining younger age groups have reported mixed results. For example, Yeung et al. [51] and Ozkaya et al. [52] examined brain stiffness in humans aged 7–18 years and found no significant variation in stiffness with age, which is consistent with the findings of Sack et al. [46] for the 18–25 age group and Takamura et al. [50] for the 20–40 age group. Conversely, McIlvain et al. [53] reported a significant increase in stiffness in the cerebellum, parietal, and temporal lobes when comparing 12–14 year olds with 18–33 year olds, while also noting a decrease in stiffness in the caudate and putamen. These findings suggest that age-related changes in stiffness may exhibit regional variability, as further supported by McIlvain et al. [54]. Consequently, overlooking these regional variations could significantly affect the interpretation of the age dependence of brain stiffness. Overall, the in vivo studies with age ranges comparable to our study do not show an overall age dependence in brain stiffness, but are limited to whole brain studies.

Our results and the contradictory results in the literature emphasize the need for further studies to investigate the nonlinear mechanical age dependence of brain tissue. Moreover, the reasons for this non-linearity should be the subject of future research. In particular, the macroscopic behavior is closely related to the microstructure [45,63,82]. Further studies are therefore needed to investigate the microscopic changes with age.

5.1.1. Age-dependent anisotropy

In the present study, we investigated the anisotropic behavior of the CC region under uniaxial compression. In addition, the material parameters of the GOH model were fitted to our data using Bayesian inference. This approach allowed us to learn the behavior of the anisotropy factor, which describes the degree of anisotropy, over time. Our results showed a non-linear evolution of anisotropy over time, with the maximum observed at 6 months (S_2). In particular, at this age, axons subjected to tension (CC_{90°) showed a 245.2% higher maximum tension than axons subjected to compression (CC_{0°). The mean dispersion parameter κ at this maximum is 0.24, which is different from the isotropic behavior (0.33). In addition, the data show considerable variability, especially within S_1, highlighting the complex nature of anisotropic changes during early developmental stages. To the best of the authors' knowledge, there are no in vitro studies investigating age-dependent anisotropy of brain tissue. However, in agreement with our results, studies using DTI and FA measurements have found a non-linear age dependence [55–57]. Chen et al. [56] analyzed human DTI data from 6 to 30 years of age and found a non-linear increase in FA until a plateau is reached at 15 years of age in

women and 21 years of age in men. After the plateau, an almost constant behavior was observed. This is in agreement with the studies of Lebel et al. [55] and Beck et al. [57]. The latter examined a wider age range (18–94 years) and found a linear decrease in FA after the age of 30. In addition, Salat et al. [103] observed a linear relationship with FA in people aged 21–76 years. The non-linear trend in anisotropy observed in the present study is consistent with the reported changes in FA and provides important insights into the age-dependent mechanical properties of brain tissue.

5.1.2. Limitations of this study

A limitation of the present study is the examination of brain tissue within 18 hours post mortem. While some studies [42,104] suggest no significant effects on mechanical properties during this post-mortem period, there are contradictory results in the literature [105–107]. The choice of this time frame was made to balance practical limitations with the need for in vitro testing, as in vivo methods such as magnetic resonance elastography are not able to capture the full complexity of the mechanical response of the brain. Due to the limited availability of ages of farmed pigs, only five age groups with non-equidistant age differences could be studied in our study. Several samples were taken from each individual brain in each region. The reason for this is partly ethical, as we wanted to take as many samples as possible from each brain. Secondly, the availability of brains of different ages is limited. If fewer samples were taken per brain, the variability in the measured stress-stretch curves could be higher than in the actual samples. The Bayesian inference used classifies the existing uncertainty in the data and ensures a transparent assessment of the conclusions drawn. However, the limited number of age groups may limit the granularity of age-related trends. Future studies with a larger number of age groups could provide deeper insights into the continuous evolution of mechanical properties over the life span. Another limitation is in the choice of material models for our data-driven learning approach. We used the isotropic Ogden model and the GOH model to capture the non-linear mechanical behavior of the CC region. Although these models are widely used in biomechanics and provide a phenomenologically and physically motivated representation, they inherently simplify the complex mechanical response of brain tissue. Choosing a different model formulation could improve specificity but would compromise comparability with existing studies. Given the complexity of biomechanical experiments, tissue variability and microstructures, maintaining consistency is critical for meaningful comparisons.

6. Conclusion

In this study, we analyzed the complex relationship between age and the mechanical properties of brain tissue. Our results show a non-linear development of the compressive and tensile shear modulus. We found a pronounced stiffening during early development, which peaked at 3 years of age, followed by a subsequent decrease. This nonlinear behavior suggests a profound influence of microstructural changes during brain development on macroscopic tissue stiffness. Furthermore, our investigation of TCA and anisotropy revealed non-linear age dependencies, both peaking at 6 months of age. Understanding the age-dependence of mechanical properties is a crucial step in developing reliable computational models for simulating of surgical procedures or diseases that become more common with age. Our study emphasizes the need to further investigate the microstructural changes during aging to elucidate the underlying mechanisms that cause the changes in mechanical properties in order to make brain models more accurate in the future.

Declaration of competing interest

The authors declare that they have no known competing financial interests or personal relationships that could have appeared to influence the work reported in this paper.

CRediT authorship contribution statement

Mayra Hoppstädter: Writing – review & editing, Writing – original draft, Visualization, Investigation, Data curation, Conceptualization. **Kevin Linka:** Writing – review & editing, Writing – original draft, Visualization, Methodology, Investigation. **Ellen Kuhl:** Writing – review & editing. **Marion Schmicke:** Writing – review & editing. **Markus Böl:** Writing – review & editing, Writing – original draft, Visualization, Supervision, Project administration, Funding acquisition, Data curation, Conceptualization.

Acknowledgements

Partial support for this research was provided by the Deutsche Forschungsgemeinschaft (DFG) under Grant 404568779.

Appendix A

A1. Maximum tensile stretch $\lambda_{at,max}$ and corresponding stress $P_{at,max}$

Table 6

Table 6
Tensile stress $P_{at,max}$, by region (basal ganglia BG, corpus callosum CC and corona radiata CR), axon orientation and age group ($S_{1/2/3/4/5}$).

Age group	$\lambda_{at,max}$			$P_{at,max}$		
	BG	$CC_{0°}$	CR	BG	$CC_{0°}$	CR
S_1	1.046	1.044	1.061	0.048 ± 0.033	0.059 ± 0.035	0.087 ± 0.030
S_2	1.073	1.091	1.071	0.115 ± 0.050	0.111 ± 0.058	0.078 ± 0.034
S_3	1.155	1.146	1.069	0.135 ± 0.039	0.322 ± 0.238	0.091 ± 0.057
S_4	1.173	1.082	1.060	0.149 ± 0.033	-	0.074 ± 0.040
S_5	-	1.140	-	-	0.081 ± 0.030	-

A2. Axial compression at $\lambda_{at,min}$

Table 7

Table 7
Compressive stress $P_{ac,\lambda_{at,max}}$, by region (cortex CX, basal ganglia BG and corona radiata CR) and age.

Set	$P_{ac,\lambda_{at,min}}$		
	BG	$CC_{0°}$	CR
$\lambda_{at,min}$	1.046	1.044	1.060
S_1	0.0082	0.0090	0.0119
S_2	0.0099	0.0034	0.0117
S_3	0.0146	0.0147	0.0161
S_4	0.0066	0.0053	0.0119
S_5	0.0036	0.0039	0.0107

A3. Age relations of nonlinearity factor α

Figs. 10 and 11

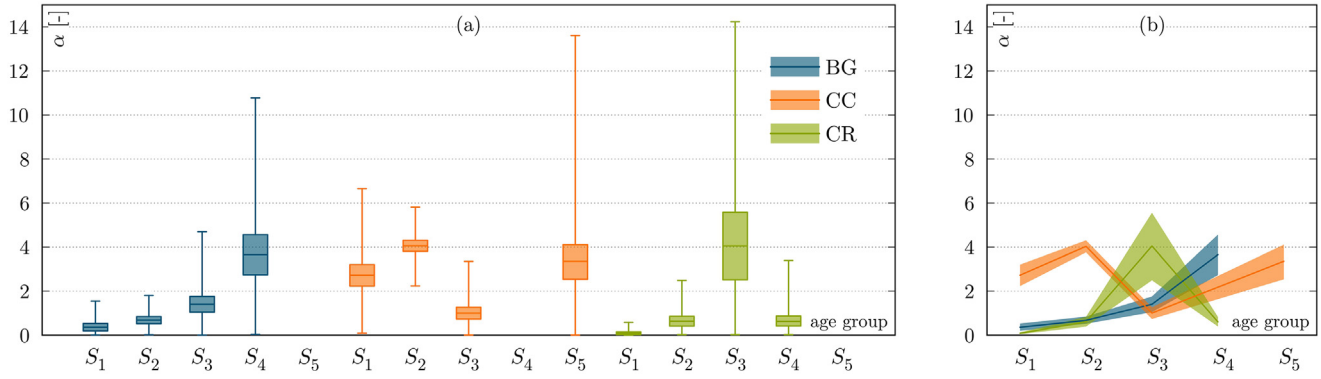

Fig. 10. Bayesian learning of the functional dependence between nonlinearity parameter and age for axial tension: (a) Hierarchically learned tensile nonlinearity parameter (α) distributions across tissue regions and age groups and (b) corresponding median nonlinearity parameter α (solid line) and percentiles (shaded areas) linearly interpolated over the tissue age.

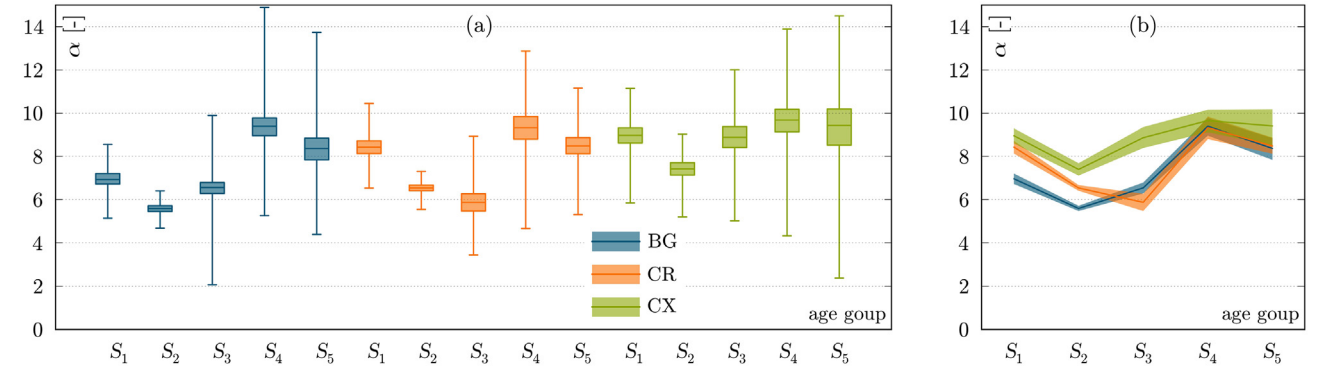

Fig. 11. Bayesian learning of the functional dependence between nonlinearity parameter and age for axial compression: (a) Hierarchically learned compressive nonlinearity parameter (α) distributions across tissue regions and age groups and (b) corresponding median nonlinearity parameter α (solid line) and percentiles (shaded areas) linearly interpolated over the tissue age.

References

[1] F.A.C. Azevedo, L.R.B. Carvalho, L.T. Grinberg, J. M. Farfel, R.E.L. Ferretti, R.E.P. Leite, W.J. Filho, R. Lent, S. Herculano-Houzel, Equal numbers of neuronal and nonneuronal cells make the human brain an isometrically scaled-up primate brain, J. Comp. Neurol. 513 (5) (2009) 532–541.

[2] S. Herculano-Houzel, The human brain in numbers: a linearly scaled-up primate brain, Front. Hum. Neurosci. (2009) 31.

[3] S. Herculano-Houzel, Scaling of brain metabolism with a fixed energy budget per neuron: implications for neuronal activity, plasticity and evolution, PLoS ONE 6 (3) (2011) e17514.

[4] B.P. Bean, The action potential in mammalian central neurons, Nat. Rev. Neurosci. 8 (6) (2007) 451–465.

[5] T.C. Südhof, Neuroligins and neurexins link synaptic function to cognitive disease, Nature 455 (7215) (2008) 903–911.

[6] G. Buzsáki, C.A. Anastassiou, C. Koch, The origin of extracellular fields and currents — EEG, ECog, LFP and spikes, Nat. Rev. Neurosci. 13 (6) (2012) 407–420.

[7] T.A. Gennarelli, L.E. Thibault, J.H. Adams, D.I. Graham, C.J. Thompson, R.P. Marcincin, Diffuse axonal injury and traumatic coma in the primate, Ann. Neurol. 12 (6) (1982) 564–574.

[8] M.P. Alexander, Mild traumatic brain injury, Neurology 45 (7) (1995) 1253–1260.

[9] M. Inglese, S. Makani, G. Johnson, B.A. Cohen, J.A. Silver, O. Gonen, R.I. Grossman, Diffuse axonal injury in mild traumatic brain injury: a diffusion tensor imaging study, J. Neurosurg. 103 (2) (2005) 298–303.

[10] V.E. Johnson, W. Stewart, D.H. Smith, Axonal pathology in traumatic brain injury, Exp. Neurol. 246 (2013) 35–43.

[11] M.S. Samuel, J.I. Lopez, E.J. McGhee, D.R. Croft, D. Strachan, P. Timpson, J. Munro, E. Schröder, J. Zhou, V.G. Brunton, N. Barker, H. Clevers, O.J. Sansom, K.I. Anderson, V.M. Weaver, M.F. Olson, Actomyosin-mediated cellular tension drives increased tissue stiffness and beta-catenin activation to induce epidermal hyperplasia and tumor growth, Cancer Cell 19 (6) (2011) 776–791.

[12] K. Pogoda, L.K. Chin, P.C. Georges, F.J. Byfield, R. Bucki, R. Kim, M. Weaver, R.G. Wells, C. Marcinkiewicz, P.A. Janmey, Compression stiffening of brain and its effect on mechanosensing by glioma cells, New J. Phys. 16 (2014) 075002.

[13] C. Wang, X. Tong, F. Yang, Bioengineered 3d brain tumor model to elucidate the effects of matrix stiffness on glioblastoma cell behavior using PEG-based hydrogels, Mol. Pharm. 11 (7) (2014) 2115–2125.

[14] M. Grujicic, G. Arakere, T. He, Material–modeling and structural–mechanics aspects of the traumatic brain injury problem, Multidiscip. Model. Mater.Struct. 6 (3) (2010) 335–363.

[15] S. Chatelin, C. Deck, F. Renard, S. Kremer, C. Heinrich, J.P. Armspach, R. Willinger, Computation of axonal elongation in head trauma finite element simulation, J. Mech. Behav. Biomed. Mater. 4 (8) (2011) 1905–1919.

[16] R.J.H. Cloots, J.A.W.v. Dommelen, M.G.D. Geers, A tissue-level anisotropic criterion for brain injury based on microstructural axonal deformation, J. Mech. Behav. Biomed. Mater. 5 (1) (2012) 41–52.

[17] C. Giordano, R.J.H. Cloots, J.A.W.v. Dommelen, S. Kleiven, The influence of anisotropy on brain injury prediction, J. Biomech. 47 (5) (2014) 1052–1059.

[18] J. Weickenmeier, C.A.M. Butler, P.G. Young, A. Goriely, E. Kuhl, The mechanics of decompressive craniectomy: personalized simulations, Comput. Methods Appl. Mech. Eng. 314 (2017) 180–195.

[19] K. Miller, G.R. Joldes, G. Bourantas, S.K. Warfield, D.E. Hyde, R. Kikinis, A. Wittek, Biomechanical modeling and computer simulation of the brain during neurosurgery, Int. J. Numer. Method Biomed. Eng. 35 (10) (2019) e3250.

[20] S. Chatelin, A. Constantinesco, R. Willinger, Fifty years of brain tissue mechanical testing: from in vitro to in vivo investigations, Biorheology 47 (5–6) (2010) 255–276.

[21] K. Miller, K. Chinzei, Constitutive modelling of brain tissue: experiment and theory, J. Biomech. 30 (11) (1997) 1115–1121.

[22] X. Jin, F. Zhu, H. Mao, M. Shen, K.H. Yang, A comprehensive experimental study on material properties of human brain tissue, J. Biomech. 46 (16) (2013) 2795–2801.

[23] Z. Li, H. Yang, G. Wang, X. Han, S. Zhang, Compressive properties and constitutive modeling of different regions of 8-week-old pediatric porcine brain under large strain and wide strain rates, J. Mech. Behav. Biomed. Mater. 89 (2019) 122–131.

[24] K. Miller, K. Chinzei, Mechanical properties of brain tissue in tension, J. Biomech. 35 (4) (2002) 483–490.

[25] T.P. Prevost, A. Balakrishnan, S. Suresh, S. Socrate, Biomechanics of brain tissue, Acta Biomater. 7 (1) (2011) 83–95.

[26] B. Rashid, M. Destrade, M.D. Gilchrist, Mechanical characterization of brain tissue in compression at dynamic strain rates, J. Mech. Behav. Biomed. Mater. 10 (2012) 23–38.

[27] B. Rashid, M. Destrade, M.D. Gilchrist, Mechanical characterization of brain tissue in tension at dynamic strain rates, J. Mech. Behav. Biomed. Mater. 33 (2014) 43–54.

[28] S. Budday, G. Sommer, C. Birkl, C. Langkammer, J. Haybaeck, J. Kohnert, M. Bauer, F. Paulsen, P. Steinmann, E. Kuhl, G.A. Holzapfel, Mechanical characterization of human brain tissue, Acta Biomater. 48 (2017) 319–340.

[29] R. Wang, M. Sarntinoranont, Biphasic analysis of rat brain slices under creep indentation shows nonlinear tension-compression behavior, J. Mech. Behav. Biomed. Mater. 89 (2019) 1–8.

[30] F. Eskandari, M. Shafieian, M.M. Aghdam, K. Laksari, Tension strain-softening and compression strain-stiffening behavior of brain white matter, Ann. Biomed. Eng. 49 (1) (2021) 276–286.

[31] M.T. Prange, S.S. Margulies, Regional, directional, and age-dependent properties of the brain undergoing large deformation, J. Biomech. Eng. 124 (2) (2002) 244–252.

[32] F. Velardi, F. Fraternali, M. Angelillo, Anisotropic constitutive equations and experimental tensile behavior of brain tissue, Biomech. Model. Mechanobiol. 5 (1) (2006) 53–61.

[33] S. Chatelin, J. Vappou, S. Roth, J.S. Raul, R. Willinger, Towards child versus adult brain mechanical properties, J. Mech. Behav. Biomed. Mater. 6 (2012) 166–173.

[34] J.D. Finan, B.S. Elkin, E.M. Pearson, I.L. Kalbian, B. Morrison, Viscoelastic properties of the rat brain in the sagittal plane: effects of anatomical structure and age, Ann. Biomed. Eng. 40 (1) (2012) 70–78.

[35] D.E. Koser, E. Moeendarbary, J. Hanne, S. Kuerten, K. Franze, CNS Cell distribution and axon orientation determine local spinal cord mechanical properties, Biophys. J. 108 (9) (2015) 2137–2147.

[36] F. Pervin, W.W. Chen, Dynamic mechanical response of bovine gray matter and white matter brain tissues under compression, J. Biomech. 42 (6) (2009) 731–735.

[37] D.B. MacManus, B. Pierrat, J.G. Murphy, M.D. Gilchrist, Region and species dependent mechanical properties of adolescent and young adult brain tissue, Sci. Rep. 7 (1) (2017) 13729.

[38] Y. Feng, R.J. Okamoto, R. Namani, G.M. Genin, P.V. Bayly, Measurements of mechanical anisotropy in brain tissue and implications for transversely isotropic material models of white matter, J. Mech. Behav. Biomed. Mater. 23 (2013) 117–132.

[39] Y. Feng, C.H. Lee, L. Sun, S. Ji, X. Zhao, Characterizing white matter tissue in large strain via asymmetric indentation and inverse finite element modeling, J. Mech. Behav. Biomed. Mater. 65 (2017) 490–501.

[40] J. Weickenmeier, S. Budday, T.C. Ovaert, E. Kuhl, R. de rooij, The mechanical importance of myelination in the central nervous system, J. Mech. Behav. Biomed. Mater. 76 (2017) 119–124.

[41] H. Gray, W.H. Lewis, Anatomy of the human body, 2000. Bartleby.com, New York, 20th ed. edition ISBN 9781587341021.

[42] S. Budday, P. Steinmann, E. Kuhl, Physical biology of human brain development, Front. Cell. Neurosci. 9 (2015) 257.

[43] J.W.T. Dickerson, J. Dobbing, R.A. McCance, Prenatal and postnatal growth and development of the central nervous system of the pig, Proc. R. Soc. London Ser. B Biol. Sci. 166 (1005) (1967) 384–395.

[44] A.S. Dekaban, D. Sadowsky, Changes in brain weights during the span of human life: relation of brain weights to body heights and body weights, Ann. Neurol. 4 (4) (1978) 345–356.

[45] S. Budday, E. Kuhl, Modeling the life cycle of the human brain, Current Opinion in Biomedical Engineering 15 (2020) 16–25.

[46] I. Sack, K.J. Streitberger, D. Krefting, F. Paul, J. Braun, The influence of physiological aging and atrophy on brain viscoelastic properties in humans, PLoS ONE 6 (9) (2011) e23451.

[47] A. Arani, M.C. Murphy, K.J. Glaser, A. Manduca, D.S. Lake, S.A. Kruse, C.R. Jack, R.L. Ehman, J. Huston, Measuring the effects of aging and sex on regional brain stiffness with MR elastography in healthy older adults, Neuroimage 111 (2015) 59–64.

[48] L.V. Hiscox, C.L. Johnson, M.D.J. McGarry, M. Perrins, A. Littlejohn, E.J.R. van Beek, N. Roberts, J.M. Starr, High-resolution magnetic resonance elastography reveals differences in subcortical gray matter viscoelasticity between young and healthy older adults, Neurobiol. Aging 65 (2018) 158–167.

[49] P. Kalra, B. Raterman, X. Mo, A. Kolipaka, Magnetic resonance elastography of brain: comparison between anisotropic and isotropic stiffness and its correlation to age, Magn. Reson. Med. 82 (2) (2019) 671–679.

[50] T. Takamura, U. Motosugi, Y. Sasaki, T. Kakegawa, K. Sato, K. J. Glaser, R.L. Ehman, H. Onishi, Influence of age on global and regional brain stiffness in young and middle-aged adults, J. Magn. Reson. Imaging 51 (3) (2019) 727–733.

[51] J. Yeung, L. Jugé, A. Hatt, L.E. Bilston, Paediatric brain tissue properties measured with magnetic resonance elastography, Biomech. Model. Mechanobiol. 18 (5) (2019) 1497–1505.

[52] E. Ozkaya, G. Fabris, F. Macruz, Z.M. Suar, J. Abderezaei, B. Su, K. Laksari, L. Wu, D.B. Camarillo, K.B. Pauly, M. Wintermark, M. Kurt, Viscoelasticity of children and adolescent brains through MR elastography, J. Mech. Behav. Biomed. Mater. 115 (2021) 104229.

[53] G. McIlvain, H. Schwarb, N.J. Cohen, E.H. Telzer, C.L. Johnson, Mechanical properties of the in vivo adolescent human brain, Dev. Cogn. Neurosci. 34 (2018) 27–33.

[54] G. McIlvain, J.M. Schneider, M.A. Matyi, M.D.J. McGarry, Z. Qi, C.L. Johnson, J.m. spielberg, Mapping brain mechanical property maturation from childhood to adulthood, Neuroimage 263 (2022) 119590.

[55] C. Lebel, L. Walker, A. Leemans, L. Phillips, C. Beaulieu, Microstructural maturation of the human brain from childhood to adulthood, Neuroimage 40 (3) (2008) 1044–1055.

[56] Z. Chen, H. Zhang, P.A. Yushkevich, M. Liu, C. Beaulieu, Maturation along white matter tracts in human brain using a diffusion tensor surface model tract-specific analysis, Front. Neuroanat. 10 (9) (2016).

[57] D. Beck, I.I. Maximov, G. Richard, O.A. Andreassen, L.T. Westlye, A.m.g. de lange, White matter microstructure across the adult lifespan: a mixed lon-

gitudinal and cross-sectional study using advanced diffusion models and brain-age prediction, Neuroimage 224 (2021) 117441.
[58] A.C. Duhaime, S.S. Margulies, S.R. Durham, M.M. O'.Rourke, J.A. Golden, S. Marwaha, R. Raghupathi, Maturation-dependent response of the piglet brain to scaled cortical impact, J. Neurosurg. 93 (3) (2000) 455–462.
[59] A. Gefen, N. Gefen, Q. Zhu, R. Raghupathi, S.S. Margulies, Age-dependent changes in material properties of the brain and braincase of the rat, J. Neurotrauma 20 (11) (2003) 1163–1177.
[60] B.S. Elkin, A. Ilankovan, B.I. Morrison, Age-dependent regional mechanical properties of the rat hippocampus and cortex, J. Biomech. Eng. 132 (1) (2010).
[61] B.S. Elkin, A.I. Ilankovan, B. Morrison, A detailed viscoelastic characterization of the p17 and adult rat brain, J. Neurotrauma 28 (11) (2011) 2235–2244.
[62] A.V. Shulyakov, S.S. Cenkowski, R.J. Buist, M.r. del bigio, Age-dependence of intracranial viscoelastic properties in living rats, J. Mech. Behav. Biomed. Mater. 4 (3) (2011) 484–497.
[63] N. Antonovaite, L.A. Hulshof, E.M. Hol, W.J. Wadman, D. Iannuzzi, Viscoelastic mapping of mouse brain tissue: relation to structure and age, J. Mech. Behav. Biomed. Mater. 113 (2021) 104159.
[64] K.L. Thibault, S.S. Margulies, Age-dependent material properties of the porcine cerebrum: effect on pediatric inertial head injury criteria, J. Biomech. 31 (12) (1998) 1119–1126.
[65] H. Mohsen, E.S.A. El-Dahshan, E.S.M. El-Horbaty, A.B.M. Salem, Classification using deep learning neural networks for brain tumors, Future Comput. Inf. J. 3 (1) (2018) 68–71.
[66] J. Ker, Y. Bai, H.Y. Lee, J. Rao, L. Wang, Automated brain histology classification using machine learning, J. Clin. Neurosci. 66 (2019) 239–245.
[67] D. Zhang, G. Huang, Q. Zhang, J. Han, J. Han, Y. Yu, Cross-modality deep feature learning for brain tumor segmentation, Pattern Recognit. 110 (2021) 107562.
[68] S. Sarraf, G. Tofighi, Deep learning-based pipeline to recognize alzheimer's disease using fMRI data, in: 2016 Future Technologies Conference (FTC), 2016, pp. 816–820.
[69] O. González-Velasco, D. Papy-García, G.L. Douaron, J.M. Sánchez-Santos, J. de Las Rivas, Transcriptomic landscape, gene signatures and regulatory profile of aging in the human brain, Biochim. Biophys. Acta (BBA) Gene Regul. Mech. 1863 (6) (2020) 194491.
[70] J.L. Webb, S.M. Moe, A.K. Bolstad, E.M. McNeill, Identification of conserved transcriptome features between humans and drosophila in the aging brain utilizing machine learning on combined data from the NIH sequence read archive, PLoS ONE 16 (8) (2021) e0255085.
[71] L. Bellantuono, L. Marzano, M. La Rocca, D. Duncan, A. Lombardi, T. Maggipinto, A. Monaco, S. Tangaro, N. Amoroso, R. Bellotti, Predicting brain age with complex networks: from adolescence to adulthood, Neuroimage 225 (2021) 117458.
[72] O.A. Zoubi, C.K. Wong, R.T. Kuplicki, H.W. Yeh, A. Mayeli, H. Refai, M. Paulus, J. Bodurka, Predicting age from brain EEG signals—a machine learning approach, Front. Aging Neurosci. 10 (2018) 184. ISSN 1663-4365
[73] S. Madireddy, B. Sista, K. Vemaganti, A bayesian approach to selecting hyperelastic constitutive models of soft tissue, Comput. Methods Appl. Mech. Eng. 291 (2015) 102–122.
[74] S. Madireddy, B. Sista, K. Vemaganti, Bayesian calibration of hyperelastic constitutive models of soft tissue, J. Mech. Behav. Biomed. Mater. 59 (2016) 108–127.
[75] P.T. Brewick, K. Teferra, Uncertainty quantification for constitutive model calibration of brain tissue, J. Mech. Behav. Biomed. Mater. 85 (2018) 237–255.
[76] L.A. Mihai, T.E. Woolley, A. Goriely, Stochastic isotropic hyperelastic materials: constitutive calibration and model selection, Proc. R. Soc. A Math. Phys. Eng. Sci. 474 (2211) (2018) 20170858.
[77] K. Teferra, P.T. Brewick, A bayesian model calibration framework to evaluate brain tissue characterization experiments, Comput. Methods Appl. Mech. Eng. 357 (2019) 112604.
[78] L. Liang, M. Liu, W. Sun, A deep learning approach to estimate chemically-treated collagenous tissue nonlinear anisotropic stress-strain responses from microscopy images, Acta Biomater. 63 (2017) 227–235.
[79] K. Linka, N. Reiter, J. Würges, M. Schicht, L. Bräuer, C.J. Cyron, F. Paulsen, S. Budday, Unraveling the local relation between tissue composition and human brain mechanics through machine learning, Front. Bioeng. Biotechnol. 9 (2021) 704738.
[80] P. Sauleau, E. Lapouble, D. Val-Laillet, C.H. Malbert, The pig model in brain imaging and neurosurgery, Animal 3 (8) (2009) 1138–1151.
[81] J. Weickenmeier, M. Kurt, E. Ozkaya, M. Wintermark, K.B. Pauly, E. Kuhl, Magnetic resonance elastography of the brain: acomparison between pigs and humans, J. Mech. Behav. Biomed. Mater. 77 (2018) 702–710.
[82] M. Hoppstädter, D. Püllmann, R. Seydewitz, E. Kuhl, M. Böl, Correlating the microstructural architecture and macrostructural behaviour of the brain, Acta Biomater. 151 (2022) 379–395.
[83] R.W. Ogden, Large deformation isotropic elasticity–on the correlation of theory and experiment for incompressible rubberlike solids, Proc. R. Soc. London. A Math. Phys. Sci. 326 (1567) (1972) 565–584.
[84] T.C. Gasser, R.W. Ogden, G.A. Holzapfel, Hyperelastic modelling of arterial layers with distributed collagen fibre orientations, J. R. Soc. Interface 3 (6) (2005) 15–35.
[85] W.R. Gilks, S. Richardson, D. Spiegelhalter, Markov Chain Monte Carlo in Practice, CRC press, 1995. ISBN 1482214970
[86] C.P. Robert, G. Casella, Monte Carlo Statistical Methods, Springer, 2010.
[87] K.L. Lange, J.A.L. Roderick, M.G.T. Jeremy, Robust statistical modeling using the t distribution, J. Am. Stat. Assoc. 84 (408) (1989) 881–896.
[88] M.D. Hoffman, A. Gelman, The no-u-turn sampler: adaptively setting path lengths in hamiltonian monte carlo, J. Mach. Learn. Res. 15 (1) (2014) 1593–1623.
[89] S. Duane, A.D. Kennedy, B.J. Pendleton, D. Roweth, Hybrid monte carlo, Phys. Lett. B 195 (2) (1987) 216–222.
[90] J. Salvatier, T.V. Wiecki, C. Fonnesbeck, C. Elkan, Probabilistic programming in python using pyMC3, PeerJ Comput. Sci. 2 (2016) e55.
[91] M. Böl, A.E. Ehret, K. Leichsenring, M. Ernst, Tissue-scale anisotropy and compressibility of tendon in semi-confined compression tests, J. Biomech. 48 (6) (2015) 1092–1098.
[92] M. Böl, K. Leichsenring, S. Kohn, A.E. Ehret, The anisotropic and region-dependent mechanical response of wrap-around tendons under tensile, compressive and combined multiaxial loads, Acta Biomater. (2024). submitted for publication
[93] M.A. Soltz, G.A. Ateshian, A conewise linear elasticity mixture model for the analysis of tension-compression nonlinearity in articular cartilage, J. Biomech. Eng. 122 (6) (2000) 576–586.
[94] S. Xie, R.J. Wallace, A. Callanan, P. Pankaj, From tension to compression: asymmetric mechanical behaviour of trabecular bone's organic phase, Ann. Biomed. Eng. 46 (6) (2018) 801–809.
[95] M. van Loocke, C.G. Lyons, C.K. Simms, A validated model of passive muscle in compression, J. Biomech. 39 (16) (2006) 2999–3009.
[96] J. Gindre, M. Takaza, K.M. Moerman, C.K. Simms, A structural model of passive skeletal muscle shows two reinforcement processes in resisting deformation, J. Mech. Behav. Biomed. Mater. 22 (2013) 84–94.
[97] M. Böl, A.E. Ehret, K. Leichsenring, C. Weichert, R. Kruse, On the anisotropy of skeletal muscle tissue under compression, Acta Biomater. 10 (7) (2014) 3225–3234.
[98] M. Böl, K. Leichsenring, M. Ernst, A.E. Ehret, Long-term mechanical behaviour of skeletal muscle tissue in semi-confined compression experiments, J. Mech. Behav. Biomed. Mater. 63 (2016) 115–124.
[99] M. Mohammadkhah, P. Murphy, C.K. Simms, The in vitro passive elastic response of chicken pectoralis muscle to applied tensile and compressive deformation, J. Mech. Behav. Biomed. Mater. 62 (2016) 468–480.
[100] P. Andrikakou, K. Vickraman, H. Arora, On the behaviour of lung tissue under tension and compression, Sci. Rep. 6 (1) (2016) 36642.
[101] K.M. Myers, S. Socrate, A. Paskaleva, M. House, A study of the anisotropy and tension/compression behavior of human cervical tissue, J. Biomech. Eng. 132 (2) (2010).
[102] K.M. Myers, C.P. Hendon, Y. Gan, W. Yao, K. Yoshida, M. Fernandez, J. Vink, R.J. Wapner, A continuous fiber distribution material model for human cervical tissue, J. Biomech. 48 (9) (2015) 1533–1540.
[103] D.H. Salat, D.S. Tuch, D.N. Greve, K.A.J.W. van der, N.D. Hevelone, A.K. Zaleta, B.R. Rosen, B. Fischl, S. Corkin, H.D. Rosas, A.M. Dale, Age-related alterations in white matter microstructure measured by diffusion tensor imaging, Neurobiol. Aging 26 (8) (2005) 1215–1227.
[104] D. Singh, S. Boakye-Yiadom, D.S. Cronin, Comparison of porcine brain mechanical properties to potential tissue simulant materials in quasi-static and sinusoidal compression, J. Biomech. 92 (2019) 84–91.
[105] A. Garo, M. Hrapko, J.A.W.v. Dommelen, G.W.M. Peters, Towards a reliable characterisation of the mechanical behaviour of brain tissue: the effects of post-mortem time and sample preparation, Biorheology 44 (1) (2007) 51–58.
[106] J. Vappou, E. Breton, P. Choquet, R. Willinger, A. Constantinesco, Assessment of in vivo and post-mortem mechanical behavior of brain tissue using magnetic resonance elastography, J. Biomech. 41 (14) (2008) 2954–2959.
[107] J. Weickenmeier, M. Kurt, E. Ozkaya, R. de Rooij, T.C. Ovaert, R.L. Ehman, K.B. Pauly, E. Kuhl, Brain stiffens post mortem, J. Mech. Behav. Biomed. Mater. 84 (2018) 88–98.